

# 1 Identification of neurobehavioural symptom groups based on 2 shared brain mechanisms

3  
4  
5  
6 **Authors:** Alex Ing, Ph.D.<sup>1</sup>; Philipp G. Sämann, M.D.<sup>2</sup>, Ph.D.; Congying Chu, Ph.D.<sup>1</sup>; Nicole  
7 Tay, Ph.D.<sup>1</sup>; Francesca Biondo, Ph.D.<sup>1</sup>; Gabriel Robert, M.D.<sup>1,3</sup>; Tianye Jia, Ph.D.<sup>1</sup>; Thomas  
8 Wolfers<sup>4</sup>; Sylvane Desrivieres Ph.D.<sup>1</sup>; Tobias Banaschewski M.D.; Ph.D.<sup>5</sup>; Arun L.W. Bokde  
9 Ph.D.<sup>6</sup>; Uli Bromberg Ph.D.<sup>7</sup>; Christian Büchel M.D.<sup>7,8</sup>; Patricia Conrod<sup>9,10</sup>; Tahmine Fadaei<sup>7</sup>;  
10 Herta Flor Ph.D.<sup>11,12</sup>; Vincent Frouin Ph.D.<sup>13</sup>; Hugh Garavan Ph.D.<sup>14</sup>; Philip A. Spechler,  
11 M.A.<sup>14</sup>; Penny Gowland Ph.D.<sup>15</sup>; Yvonne Grimmer<sup>5</sup>; Andreas Heinz M.D., Ph.D.<sup>16</sup>; Bernd  
12 Ittermann Ph.D.<sup>17</sup>; Viola Kappel<sup>18</sup>; Jean-Luc Martinot M.D., Ph.D.<sup>19</sup>; Andreas Meyer-  
13 Lindenberg M.D., Ph.D.<sup>20</sup>; Sabina Millenet Dipl.-Psych.<sup>5</sup>; Frauke Nees Ph.D.<sup>5,11</sup>; Betteke van  
14 Noort<sup>18</sup>; Dimitri Papadopoulos Orfanos Ph.D.<sup>13</sup>; Marie-Laure Paillère Martinot<sup>21</sup>; Jani  
15 Penttilä<sup>22</sup>; Luise Poustka M.D.<sup>23</sup>; Erin Burke Quinlan Ph.D.<sup>1</sup>; Michael N. Smolka M.D.<sup>24</sup>;  
16 Argyris Stringaris<sup>25,26</sup>; Maren Struve<sup>24</sup>; Ilya M. Veer Ph.D.<sup>16</sup>; Henrik Walter M.D., Ph.D.<sup>16</sup>;  
17 Robert Whelan Ph.D.<sup>27</sup>; Ole A. Andreassen, M.D., Ph.D.<sup>28,29</sup>; Ingrid Agartz, M.D.,  
18 Ph.D.<sup>29,30,31</sup>; Hervé Lemaitre<sup>32</sup>; Edward D. Barker<sup>33,1</sup>; John Ashburner, Ph.D.<sup>34</sup>; Elisabeth  
19 Binder M.D.<sup>2</sup>, Ph.D.; Jan Buitelaar M.D., Ph.D.<sup>4</sup>; Andre Marquand Ph.D.<sup>4</sup>; Trevor W.  
20 Robbins, Ph.D.<sup>35</sup>; Gunter Schumann M.D., Ph.D.<sup>1,36\*</sup>; IMAGEN Consortium.

## 21 Affiliations:

22  
23 <sup>1</sup> Centre for Population Neuroscience and Precision Medicine (PONS), Institute of  
24 Psychiatry, Psychology & Neuroscience, SGDP Centre, King's College London, London,  
25 United Kingdom;

26 <sup>2</sup> Neuroimaging, Max Planck Institute of Psychiatry, Munich, Germany;

27 <sup>3</sup> Behavior and Basal Ganglia research unit, University of Rennes, Rennes, France;

28 <sup>4</sup> Donders Institute for Brain, Cognition and Behaviour, Radboud University, Nijmegen, The  
29 Netherlands;

30 <sup>5</sup> Department of Child and Adolescent Psychiatry and Psychotherapy, Central Institute of  
31 Mental Health, Medical Faculty Mannheim, Heidelberg University, Mannheim, Germany;

32 <sup>6</sup> Discipline of Psychiatry, School of Medicine and Trinity College Institute of Neuroscience,  
33 Trinity College Dublin, Dublin, Ireland;

34 <sup>7</sup> Systems Neuroscience, University Medical Centre Hamburg-Eppendorf, Hamburg,  
35 Germany;

36 <sup>8</sup> Department of Psychology, Stanford University, Stanford, California USA;

37 <sup>9</sup> Department of Psychological Medicine, Institute of Psychiatry, Psychology & Neuroscience,  
38 King's College London, UK;

39 <sup>10</sup> Department of Psychiatry, Université de Montréal, CHU Ste Justine Hospital, Montreal  
40 QC, Canada;

41 <sup>11</sup> Institute of Cognitive and Clinical Neuroscience, Central Institute of Mental Health, Medical  
42 Faculty Mannheim, Heidelberg University, Mannheim, Germany;

43 <sup>12</sup> Department of Psychology, School of Social Sciences, University of Mannheim,  
44 Mannheim, Germany;

45 <sup>13</sup> NeuroSpin, CEA, Université Paris-Saclay, Gif-sur-Yvette, France;

46 <sup>14</sup> Departments of Psychiatry and Psychology, University of Vermont, Burlington, Vermont,  
47 USA;

48 <sup>15</sup> Sir Peter Mansfield Imaging Centre School of Physics and Astronomy, University of  
49 Nottingham, University Park, Nottingham, United Kingdom;

50 <sup>16</sup> Department of Psychiatry and Psychotherapy CCM, Charité – Universitätsmedizin Berlin,  
51 corporate member of Freie Universität Berlin, Humboldt-Universität zu Berlin, and Berlin  
52 Institute of Health, Berlin, Germany;

53 <sup>17</sup> Biomedical Magnetic Resonance, Physikalisch-Technische Bundesanstalt (PTB),  
54 Braunschweig and Berlin, Germany;

55 <sup>18</sup> Department of Child and Adolescent Psychiatry Psychosomatics and Psychotherapy,  
56 Charité, Humboldt University, Berlin, Germany;

57 <sup>19</sup> Institut National de la Santé et de la Recherche Médicale, INSERM Unit 1000  
58 “Neuroimaging & Psychiatry”, University Paris Saclay, University Paris Descartes; Dlgiteo-  
59 Labs, Gif-sur-Yvette; and Maison de Solenn, Paris, France;

60 <sup>20</sup> Department of Psychiatry and Psychotherapy, Central Institute of Mental Health, Medical  
61 Faculty Mannheim, Heidelberg University, Mannheim, Germany;

62 <sup>21</sup> Institut National de la Santé et de la Recherche Médicale, INSERM Unit 1000  
63 “Neuroimaging & Psychiatry”, University Paris Saclay, University Paris Descartes; Dlgiteo-  
64 Labs, Gif-sur-Yvette; and AP-HP.Sorbonne Université, Department of Child and Adolescent  
65 Psychiatry, Pitié-Salpêtrière Hospital, Paris, France;

66 <sup>22</sup> Department of Social and Health Care, Psychosocial Services Adolescent Outpatient  
67 Clinic, Lahti, Finland;

68 <sup>23</sup> Department of Child and Adolescent Psychiatry and Psychotherapy, University Medical  
69 Centre Göttingen, Göttingen, Germany;

70 <sup>24</sup> Department of Psychiatry and Neuroimaging Center, Technische Universität, Dresden,  
71 Dresden, Germany;

72 <sup>25</sup> Department of Child and Adolescent Psychiatry, Institute of Psychiatry, Psychology &  
73 Neuroscience, King's College London, London, United Kingdom;

74 <sup>26</sup> Mood Brain and Development Unit (MBDU), National Institute of Mental Health / NIH,  
75 Bethesda MD, USA;

76 <sup>27</sup> School of Psychology and Global Brain Health Institute, Trinity College Dublin, Dublin,  
77 Ireland;

78 <sup>28</sup> Division of Mental Health and Addiction, Oslo University Hospital, Oslo, Norway;

79 <sup>29</sup> NORMENT, Institute of Clinical Medicine, University of Oslo, Oslo, Norway;

80 <sup>30</sup> Department of Psychiatric Research, Diakonhjemmet Hospital, Oslo, Norway;

81 <sup>31</sup> Department of Clinical Neuroscience, Centre for Psychiatric Research, Karolinska  
82 Institutet, Stockholm, Sweden;

83 <sup>32</sup> Institut National de la Santé et de la Recherche Médicale, UMR 992 INSERM, CEA,  
84 Faculté de médecine, Université Paris-Sud, Université Paris-Saclay, NeuroSpin, Gif-sur-  
85 Yvette, France;

86 <sup>33</sup> Department of Psychology, Institute of Psychiatry, Psychology and Neuroscience, King's  
87 College London, London, United Kingdom;

88 <sup>34</sup> Wellcome Centre for Human Neuroimaging, UCL Institute of Neurology, University College  
89 London, London, United Kingdom;

90 <sup>35</sup> Department of Psychology and Behavioural and Clinical Neuroscience Institute, University  
91 of Cambridge, Cambridge, United Kingdom;

92 <sup>36</sup> PONS Research Group, Dept of Psychiatry and Psychotherapy, Campus Charite Mitte,  
93 Humboldt University, Berlin and Leibniz Institute for Neurobiology, Magdeburg, Germany,  
94 and Institute for Science and Technology of Brain-inspired Intelligence (ISTBI), Fudan  
95 University, Shanghai, P.R. China.

96

97

98

99

100

101

102 **Abstract:**

103 **Most psychopathological disorders develop in adolescence. The biological**  
104 **basis for this development is poorly understood. To enhance diagnostic**  
105 **characterisation, and develop improved targeted interventions, it is critical to**  
106 **identify behavioural symptom groups that share neural substrates. We ran**  
107 **analyses to find relations between behavioral symptoms, and neuroimaging**  
108 **measures of brain structure and function in adolescence. We found two**  
109 **symptom groups, consisting of anxiety/depression and executive dysfunction**  
110 **symptoms respectively, which correlated with distinct sets of brain regions**  
111 **and inter-regional connections, measured by structural and functional**  
112 **neuroimaging modalities. We found that the neural correlates of these**  
113 **symptom groups were present before behavioural symptoms had developed.**  
114 **These neural correlates showed case-control differences in corresponding**  
115 **psychiatric disorders, depression and ADHD, in independent clinical samples.**  
116 **By characterising behavioral symptom groups based on shared neural**  
117 **mechanisms, our results provide a framework for developing a classification**  
118 **system for psychiatric illness, which is based on quantitative**  
119 **neurobehavioural measures.**

120

121

122

123

124

125           Adolescence and its transition toward young adulthood is a critical period for  
126 the development of psychiatric illness with half of the lifetime psychopathological  
127 burden emerging by the mid-teens, and 75% by the mid-20s<sup>1</sup>. It coincides with major  
128 structural changes in grey and white matter<sup>2</sup> that are particularly pronounced in the  
129 limbic system and the prefrontal cortex<sup>3</sup>. Cognitive and (other) behavioural  
130 maturation reflects this brain-wide developmental process<sup>4</sup>. As psychopathological  
131 symptoms during adolescent brain re-organization are often unspecific, and in many  
132 cases reversible, it has been difficult to unambiguously identify early markers for  
133 sustained mental illness. Thus, most patients present during adulthood, often at a  
134 point when severe psychopathology has developed, which gravely impairs their daily  
135 functioning. Presentation at this advanced stage increases individual suffering and  
136 renders therapeutic interventions more difficult.

137           Currently, both adolescent and adult psychiatric diagnoses are made on the  
138 basis of combinations of behavioural symptoms that - whilst reflecting the  
139 psychopathological experience of generations of clinicians and patients - are not  
140 necessarily related to homogeneous pathophysiological or etiological processes.  
141 This results in biological heterogeneity within diagnostic entities<sup>5</sup>, high rates of  
142 comorbidity between diagnoses<sup>6,7</sup>, and ill-defined targets for drug development. This  
143 is particularly relevant in adolescence, where there is evidence to suggest that  
144 psychiatric illness is more dimensional and less categorical than adult  
145 psychopathology. Neuroimaging methods offer the opportunity to identify the  
146 biological mechanisms underpinning mental illness, without recourse to these  
147 categorisations<sup>8,9</sup>.

148           One of the challenges in breaking up diagnostic borders in favour of more  
149 homogenous clusters of symptoms sharing common neural mechanisms, is that

150 biological and behavioral data need to be combined in a meaningful way. A suitable  
151 method for this purpose is canonical correlation analysis (CCA), which is formulated  
152 to maximize the correlation between variables in two views of a dataset. This  
153 technique has previously been used to link complex behavioural datasets with  
154 functional brain networks<sup>10</sup>. However, CCA has a number of limitations: It cannot be  
155 applied to data with more features than samples, results are difficult to interpret  
156 owing to a lack of localizability, and it is only possible to find relations between two  
157 sets of variables. The first two of these issues can be addressed using sparse  
158 canonical correlation analysis (sCCA)<sup>11,12</sup>, which has been used to find modes of  
159 shared variation between resting state functional connectivity MRI, and behavioral  
160 measures in adolescents and young adults<sup>12</sup>. However, this approach is still limited  
161 in that it is only possible to identify relations between psychiatric symptoms and one  
162 kind of biological measure at a time. We further enhanced sCCA by formulating a  
163 constrained form of multiple canonical correlation analysis, which maximizes the  
164 correlation between psychiatric symptoms, and several different neuroimaging  
165 modalities simultaneously<sup>13</sup>, before combining them in a linear regression model; we  
166 term this approach sparse multiple canonical correlation analysis regression  
167 (msCCA-regression).

168 We investigated whether symptoms contributing to DSMV/ICD10 diagnoses  
169 can be reconfigured to identify 'neurobehavioral' symptom groups that best represent  
170 specific underlying dysfunctional brain networks in adolescence. Here, we used a  
171 data driven approach applied to a large general population neuroimaging sample to  
172 investigate direct relations between neuroimaging measures of brain structure and  
173 function, yet without immediate recourse to diagnostic psychiatric categories.  
174 Following this, we sought to determine whether the regions we found to be related to

175 psychiatric symptoms in adolescence were associated with fully-blown clinical  
176 psychopathology in several independent clinical samples. Overall, this multi-step  
177 approach enabled us to identify brain correlates of psychopathology in adolescence,  
178 probe their predictive value in the critical period between age 14 and age 19, and  
179 characterize these brain correlates against the development of full-blown  
180 psychopathology.

181

182

### 183 **Results**

184 We used msCCA-regression (please see the methods section under the sub-  
185 heading: Multiple Sparse Canonical Correlation Analysis Regression) to link  
186 participant responses to the Development and Well Being Assessment (DAWBA), a  
187 structured interview for psychiatric DSMV/ICD-10 diagnoses<sup>14</sup> (Supplementary Table  
188 1), with voxel-based morphometry (VBM)<sup>15</sup> measures of grey matter volume,  
189 fractional anisotropy (FA) along major white matter tracts using tract-based spatial  
190 statistics (TBSS)<sup>16</sup>, and functional connectivity between different brain regions,  
191 mapped from resting state (rs-fMRI) scans<sup>17</sup>. T<sub>1</sub> and DTI data were pre-processed  
192 using voxel-wise VBM<sup>18</sup> and TBSS<sup>19</sup> methods respectively, as these procedures  
193 have been extensively studied and applied to real data. We mapped inter-regional  
194 rs-fcMRI connections across the brain using nodal maps defined by Miller et al<sup>17</sup>,  
195 reasons for our pre-processing and analysis choices are detailed in the methods  
196 section of the paper under the sub-heading: Different Neuroimaging Pre-processing  
197 Strategies. We investigated ninety DAWBA items (symptoms) related to a broad  
198 range of psychiatric disorders, including affective and anxiety symptoms, attention  
199 deficit/hyperactivity and conduct symptoms, as well as substance use, eating

200 disorders, and symptoms of psychosis (Supplementary Table 1)<sup>14</sup>. This analysis was  
201 carried out on the general population IMAGEN sample, on participants of age 19.  
202 Following an in-depth QC (see methods under the sub-heading: IMAGEN analysis),  
203 data for n = 666 participants was available at age 19.

204 To avoid overestimating the variance shared between psychiatric symptoms,  
205 and the neuroimaging modalities analysed (overfitting), we used a train/test analysis  
206 design, which allows us to estimate effect sizes in an unbiased way. Using a test set  
207 also allowed us to carry out further characterization of the data, without running into  
208 circularity problems. We carried out model selection in a training dataset of 70% of  
209 the data (n=467), and model validation in the testing dataset of the remaining 30%  
210 (n=199). To enhance stability we resampled the data and retained only variables that  
211 contributed to the model in 90% of resamples (see methods under the sub-heading:  
212 Stability Selection, and Supplementary Figure 1)<sup>21</sup>. Demographic information on the  
213 full sample, training and testing sets is given in Supplementary Figure 2. The  
214 msCCA-regression procedure we used in this investigation is designed to maximise  
215 associations between variable-sets. For this reason, all msCCA-regression  
216 significance values reported in the text are one-sided.

217  
218 Using msCCA-regression, we found a significant relation between a subset of six  
219 DAWBA symptoms (see Figure 1), and VBM, TBSS and rs-fMRI measures  
220 ( $r=0.59(465)$ ,  $p<0.001$ ). The behavioural correlates derived from DAWBA covered  
221 symptoms linked to feelings of depression, anxiety and somatic problems, as well as  
222 temper and attentional problems (Figure 1). The model was also significant when  
223 applied to the test dataset ( $r=0.23(197)$ ,  $p<0.001$ , 95% CIs=0.13,  $\infty$ ) (Figure 1),  
224 explaining 5.30% of the variance between psychiatric symptoms and the brain. Brain



225 correlates derived from VBM, TBSS and rs-fcMRI measures were associated with  
226 this anxiety/depression symptom group with correlation values of:  $r=0.16(197)$ ,  
227  $p=0.017$ , 95% CIs= $0.040, \infty$ ;  $r =0.14(197)$ ,  $p=0.040$ , 95% CIs= $0.037, \infty$  and  
228  $r=0.15(197)$ ,  $p=0.029$ , 95% CIs= $0.041, \infty$  respectively (with all p-values FWE-  
229 corrected for multiple comparisons, see methods under the sub-heading: Analysis  
230 Design, and Supplementary Figure 3).

231 VBM, TBSS and rs-fcMRI modalities all showed an individually significant  
232 relation to psychopathology. We carried out further localization analyses in each  
233 modality to identify brain regions that showed an individually significant relation to  
234 psychopathology (see methods under the sub-heading: Additional Analyses to  
235 Localise Effects). In this localization analysis, we identified one gray matter cluster in  
236 the right inferior temporal gyrus ( $r=0.16(197)$ ,  $p=0.032$  FWE corrected, 95%  
237 CIs= $0.041, \infty$ ), and a single cluster of decreased fractional anisotropy in the genu of  
238 the corpus callosum ( $r = 0.16(197)$ ,  $p=0.031$  FWE corrected, 95% CIs= $0.041, \infty$ ).  
239 Both of these brain regions have been among those exhibiting the largest differences  
240 between healthy controls and patients with depression, in recent large, well-powered  
241 meta-analyses<sup>22,23</sup>. Further, we found an increase in functional connectivity between  
242 the default mode network, and the cerebellum ( $r=0.15(197)$ ,  $p=0.041$  FWE corrected,  
243 95% CIs= $0.037, \infty$ ); the default mode network has been implicated in several  
244 different psychiatric disorders, but depression in particular, with recent research  
245 showing that connectivity between the cerebellum and the default mode network is  
246 altered in patients with depression<sup>24</sup>. Information on the full set of regions found to be  
247 associated with psychiatric symptoms can be found in Supplementary Tables 2 and  
248 3 and Supplementary Figures 4 and 5.

249 We then removed the effects of the first canonical relation and investigated  
250 the presence of a second dimension of shared variance between symptoms and the  
251 brain (see methods under the sub-heading: Finding Multiple Modes of  
252 Variation). Here, we identified another behavioral correlate consisting of five items  
253 from the DAWBA, including: problems with attention, fidgeting, rapidly changing  
254 moods and (lack of) conscientiousness that was significantly associated with the  
255 neuroimaging modalities ( $r=0.46(465)$ ,  $p=0.004$ ). The test sample correlation is  
256 significant at ( $r=0.19(197)$ ,  $p=0.002$ , 95% CIs= $0.087, \infty$ ), explaining 3.61% of the  
257 variance between psychiatric symptoms and the brain. Brain correlates derived from  
258 VBM, TBSS and rs-fcMRI measures were associated with the executive dysfunction  
259 symptom group with correlation values of  $r=0.19(197)$ ,  $p=0.012$ , 95% CIs= $0.079, \infty$ ;  
260  $r=0.070(197)$ ,  $p=0.21$ , 95% CIs= $-0.029, \infty$  and  $r=0.020(197)$ ,  $p=0.58$ , 95% CIs= $-$   
261  $0.090, \infty$  respectively. These results are displayed in Figure 2.

262  
263 As the VBM modality was the only modality in this second canonical relation  
264 to show an individually significant relation to psychopathology, we only carried out a  
265 localization analysis for VBM data in this modality; we found that executive  
266 dysfunction symptoms correlated with a single grey matter cluster in the right middle  
267 temporal gyrus ( $r = 0.16(197)$ ,  $p = 0.024$  FWE corrected, 95% CIs= $0.049$ ), an area  
268 that has previously been shown to be associated with ADHD symptomology<sup>25</sup>.  
269 Information on the full set of regions found to be associated with psychiatric  
270 symptoms can be found in Supplementary Tables 4 and 5 and Supplementary  
271 Figures 4 and 5. Associations between canonical anxiety/depression and executive  
272 dysfunction canonical correlates are given in Supplementary Table 6. Our results  
273 were robust to different rs-fcMRI atlas choices, as shown by repeated analyses using

274 a different nodal definition<sup>20</sup>, which generated similar results (Supplementary Figure  
275 6).

276

277

### 278 **Hypothesis Driven Analysis**

279 To determine if the canonical symptom groups identified in our data-driven analysis  
280 show a stronger relation to neuroimaging measures than existing means of  
281 organizing psychiatric symptoms, we carried out a hypothesis driven analysis using  
282 internalizing and externalizing symptoms, which are often used in adolescent  
283 psychiatric diagnostics. We tested whether the canonical symptom groups identified  
284 with msCCA-regression were able to explain more variance than this widely used  
285 model of illness (see methods under the sub heading: Hypothesis Driven Analysis)<sup>26</sup>.

286 We term these pre-defined symptom groups as DAWBA-internalising and DAWBA-  
287 externalising. We found that the correlation of the DAWBA-internalising dimension of  
288 psychopathology with neuroimaging measures only shows trend-level significance in  
289 the test set ( $r=0.12(197)$ ,  $p=0.060$ , 95% CIs= $-0.02, \infty$ ) and explains 1.9% of variance.

290 Similarly, DAWBA-externalising dimensions of psychiatric illness correlated with  
291 neuroimaging measures at ( $r=0.040(197)$ ,  $p=0.28$ , 95% CIs= $-0.095, \infty$ ) in the test  
292 set, explaining 0.16% of the variance (Supplementary Figure 7). We then used a  
293 modified version of Dunn and Clarke's  $z^{27,28}$  to test directly whether the association  
294 of the canonical symptom groups with the brain was significantly stronger than their  
295 pre-defined analogues. While the symptom-brain correlation of the executive-  
296 dysfunction symptom group was indeed significantly stronger than that of the  
297 DAWBA-externalizing symptom group ( $Z=1.95(196)$ ,  $p = 0.029$ ), we did not find  
298 evidence that the strength of the association between the anxiety/depression

299 symptom group and the brain was significantly larger than that of the DAWBA-  
300 internalizing group ( $Z=0.92(196)$ ,  $p = 0.18$ ).

301

### 302 **Longitudinal Analysis**

303 We carried out the initial cross-sectional analysis relating psychiatric symptoms to  
304 brain at age 19, as most psychopathological symptoms will have become manifest  
305 by this age. To investigate how adolescent brain development relates to the  
306 development of psychopathological symptoms, we analyzed data from the same  
307 participants at age 14 years. First, we repeated the cross-sectional msCCA-  
308 regression analysis using VBM and TBSS (rsfMRI data was not available at age 14).  
309 We found a non-significant, trend level association between symptoms and  
310 neuroimaging measures of  $r = 0.42(410)$ ,  $p = 0.11$  in the training set. We found  
311 similarly non-significant results in the testing set ( $r = 0.10(180)$ ,  $p = 0.090$ , 95% CIs=  
312  $0.017, \infty$ ). The results of these analyses are displayed in Supplementary Figure 8.

313 There is previous evidence to suggest that neuroimaging measures precede the  
314 development of psychiatric symptoms in adolescence<sup>29</sup>. We tested whether that was  
315 the case with the canonical symptom groups established in the present study by  
316 extracting the TBSS and VBM regions discovered at age 19 and using them as  
317 regions of interest at age 14. In order to obtain unbiased estimates of effect, we  
318 looked for associations in the test sample. After a conservative quality control  
319 procedure (see methods under the sub-headings: Longitudinal Analysis),  $n = 182$   
320 participants were available for analysis at this time-point. Our data did not show any  
321 evidence of an association between anxiety/depression brain correlates and  
322 anxiety/depression symptoms at 14 years  $r=0.020(180)$ ,  $p=0.40$ , 95% CIs= $-0.10, \infty$ .  
323 However, the brain correlates taken from data at age 14, were predictive of

324 symptoms at age 19  $r=0.14(180)$ ,  $p=0.023$ , 95% CIs= $0.022, \infty$ . These results are  
325 shown in figure 3. The difference in correlation between brain correlates at age 14  
326 years with anxiety/depression symptoms at 14 years and 19 years was also  
327 significant, testing for a difference in association using a modified version of Dunn  
328 and Clarke's Z ( $Z=1.74(179)$ ,  $p=0.041$ )<sup>28</sup>. We did not find evidence of an association  
329 between brain correlates and symptoms of executive dysfunction at age 14 years  
330 ( $r=0.030(180)$ ,  $p=0.41$ , 95% CIs= $-0.093, \infty$ ). Prediction of symptoms at 19 years  
331 showed a trend towards significance ( $r=0.11(180)$ ,  $p=0.065$ , 95% CIs = $-0.010, \infty$ ).

332

333

334

335

### 336 **Clinical Characterization**

337 We investigated whether the canonical correlates of psychopathology we identified in  
338 a general population adolescent sample are correlated with fully developed  
339 psychiatric illnesses. In these analyses, we looked for case-control differences in the  
340 anxiety/depression and executive dysfunction canonical correlates, across four  
341 common psychiatric illnesses in several independent clinical samples. We carried out  
342 these analyses using VBM data alone, as this was the only data modality that  
343 showed an individually significant association with both symptom groups. Clinical  
344 and demographic information associated with the different clinical samples is  
345 displayed in Supplementary Figure 9 and Supplementary tables 7-9. Extensive  
346 information on quality control and data exclusion criteria for these clinical samples is  
347 given in the methods section of this paper following the sub-heading: Clinical

348 Analyses. In assessing this data, we were looking for a directional effect, we  
349 therefore report significance levels resulting from one-tailed tests in this section of  
350 the paper.

351 When analyzing the data for case-control differences in grey matter correlates  
352 of anxiety/depression symptoms, we found significant reductions in regional grey  
353 matter volume in independent samples of patients with Depression (t-  
354 statistic=4.61(612),  $p < 0.001$ , Cohen's  $D = 0.39$ , 95% CIs=0.25,  $\infty$ ), Schizophrenia (t-  
355 statistic=2.54(445),  $p = 0.002$ , Cohen's  $D = 0.25$ , 95% CIs = 0.087,  $\infty$ ) and in ADHD (t-  
356 statistic=1.84(203),  $p = 0.034$ , Cohen's  $D = 0.26$ , 95% CIs=0.030,  $\infty$ ). In the executive  
357 dysfunction grey matter correlates, we found significant differences between patients  
358 and healthy controls in ADHD (t-statistic=2.19(203),  $p = 0.014$ , Cohen's  $D = 0.32$ , 95%  
359 CIs=0.070,  $\infty$ ), Schizophrenia (t-statistic=2.84(445),  $p = 0.0026$ , Cohen's  $D = 0.28$ , 95%  
360 CIs=0.11,  $\infty$ ) and Depression (t-statistic=1.65(612),  $p = 0.050$ , Cohen's  $D = 0.14$ , 95%  
361 CIs=0.001,  $\infty$ ). We did not find significant effects of bipolar disorder along either of  
362 these dimensions (t-statistic=-0.23(473),  $p = 0.59$ , Cohen's  $D = -0.02$ , 95% CIs=-0.17,  
363  $\infty$ ) and (t-statistic=-1.33(473),  $p = 0.90$ , Cohen's  $D = -0.12$ , 95% CIs=-0.27,  $\infty$ )  
364 respectively (Figure 4). In these case-control analyses, the data distribution was  
365 assumed to be normal but this was not formally tested. To test whether the observed  
366 reduction in grey matter was specific to the brain correlates identified, as opposed to  
367 being a proxy for a generalized, brain-wide reduction in grey matter, we repeated the  
368 clinical comparisons using total grey matter as a covariate of no interest in addition  
369 to total intracranial volume (Supplementary Figure 10). ADHD and Depression  
370 results were unaffected by this change in pre-processing. In contrast, the  
371 Schizophrenia results were no longer significant.

372  
373

374

375 **Discussion**

376 We ran analyses to establish direct relations between psychiatric symptoms and  
377 neuroimaging measures of brain structure and function, without immediate reference  
378 to pre-defined psychiatric categories. This kind of dimensional, data-driven,  
379 approach is particularly relevant in adolescence where there is a good deal of  
380 evidence suggesting that psychopathology is less differentiated than in adulthood  
381 and therefore doesn't fit into the traditional categorical conception of psychiatric  
382 disorder<sup>30,31</sup>. We find two largely non-overlapping sets of brain regions that correlate  
383 with different sets of psychiatric symptoms. The first symptom dimension  
384 predominantly encompassed anxiety/depression symptoms whilst the second  
385 dimension mainly consisted of executive dysfunction symptoms.

386 The anxiety/depression canonical symptom correlate was significantly associated  
387 with T<sub>1</sub>, rs-fcMRI and DTI data modalities. Participants scoring highly on this  
388 psychiatric scale showed decreased grey matter volume in the middle temporal  
389 gyrus, reduced fractional anisotropy in the genu of the corpus callosum, and  
390 increased functional connectivity between the default mode network and the  
391 cerebellum. A recent meta-analysis has demonstrated an association of depression  
392 with the right inferior temporal gyrus<sup>22</sup>, a region exhibiting close connections with the  
393 limbic system, consistent with the theory that depression results from dysfunctional  
394 cortico-limbic circuits<sup>32</sup>. The genu of the corpus callosum is a commissural white  
395 matter pathway that links left and right prefrontal brain regions<sup>33</sup>. Changes in the  
396 structure of the corpus callosum are known to result in altered inter-hemispheric  
397 connectivity and impaired emotional control<sup>34</sup>. The genu of the corpus callosum has  
398 been shown to be the white matter region with the largest difference in FA between

399 controls and patients with major depression<sup>35</sup>. The default-mode network is a set of  
400 brain regions that reliably exhibit a decrease in activity when the brain is engaged in  
401 non-self-directed tasks; this network is thought to be primarily responsible for self-  
402 inspection and internal monitoring<sup>36,37</sup>, which are processes overactive in  
403 depression<sup>38</sup>. Increased connectivity between the default-mode network and the  
404 cerebellum has been previously reported in drug-naive depressive patients<sup>24</sup>,  
405 consistent with its recently discovered involvement in complex cognitive and  
406 emotional processes<sup>39</sup>.

407 We found that the executive dysfunction psychiatric symptom group was significantly  
408 correlated with neuroimaging measures derived from T<sub>1</sub> data. Here, decreased grey  
409 matter was localised to the Right Middle Temporal Gyrus, previously linked to  
410 ADHD<sup>25</sup>. These results are more difficult to interpret as the function of this brain area  
411 is not well studied. As with the rest of the temporal lobe, this brain area is thought to  
412 be responsible for generating meaning from sensory inputs<sup>19</sup>. Further, the temporal  
413 lobe functions in close relation with the hippocampus in the formation of memories<sup>19</sup>.  
414 Therefore, atrophied grey matter in this brain area may help explain the learning  
415 deficits often observed with ADHD-like symptoms.

416 The identification of brain systems from a population-based cohort that is not  
417 suffering from any other psychiatric illness has major advantages: By identifying sub-  
418 clinical correlates of psychiatric illness, prior to the full manifestation of disorder, it is  
419 possible to avoid the potential impact of effects indirectly related to illness, such as  
420 substance use and medication effects. For example, 17% percent of the  
421 schizophrenia, and 21% percent of the Bipolar samples but none of the healthy  
422 controls studied here have a history of alcohol abuse, which has been linked to  
423 widespread decreases in grey matter<sup>40</sup>. In addition, various psychiatric medicines,



424 including lithium, which is often prescribed to Bipolar patients, have also been linked  
425 to alterations in grey matter volume<sup>41</sup>, it is possible that lithium-induced increases in  
426 grey matter volume may have contributed to the observed absence of significant  
427 findings in Bipolar patients in this study.

428 We compared the efficacy of the data-driven msCCA-regression method with  
429 pre-defined psychiatric scales of internalising and externalising symptoms. We found  
430 that the data driven approach identified relations between symptoms and the brain  
431 that were significantly stronger than a similar approach using standard internalising  
432 and externalising psychiatric symptom scales, defined without reference to any  
433 underlying biology. The fact that the canonical symptom groups show a stronger  
434 correlation with neuroimaging measures than pre-defined scales is important as it  
435 shows that data driven methods may offer the potential to refine existing psychiatric  
436 categorisations<sup>6</sup>.

437 It is notable that grey matter correlates of psychopathology are already  
438 present at age 14 years, preceding the development of symptoms that only become  
439 manifest 5 years later, at 19 years. We also found that the brain correlates  
440 identified in the adolescent general population replicate in independent clinical  
441 samples of corresponding psychiatric disorders, namely depression and ADHD. In  
442 addition to validating our primary results gained from population cohorts, these  
443 results raise the prospect of using neuroimaging measures, discovered in preclinical  
444 samples, as predictors of future psychopathology, thus enabling the development of  
445 targeted interventions in a young age group, where such measures are most  
446 effective in reducing the burden of mental illness<sup>42</sup>.

447 It is important to note that the results of the msCCA-regression analysis  
448 applied here, depend on the distribution of prevalence of psychopathological

449 symptoms in each sample investigated. Thus, while a general population sample  
450 may yield an index of the normative variance in psychiatric symptoms from  
451 a broader range of different psychiatric disorders and their neural correlates, a  
452 patient sample might yield a narrower biological stratification within distinct clinical  
453 psychiatric categories, e.g. different biotypes of depression<sup>5</sup>, or symptoms  
454 of psychosis.

455 By basing symptom groups upon brain correlates, and by demonstrating  
456 specific associations of these correlates with clinical psychopathology, we have  
457 characterized stratification markers based on shared neural substrates. By  
458 discovering that these brain correlates identified in young adults are already  
459 established during adolescence, we have characterized biological risk markers prior  
460 to the manifestation of symptoms. Our work thus shows how major obstacles can be  
461 overcome in developing a taxonomy for psychiatric illness based on quantifiable  
462 neurobehavioral phenotypes.

463

464

465

466

467

468

469

470

471

472

473

474

475

476

477

478

479

480 **Methods**

481 **Ethics Statement**

482 **IMAGEN**

483 Each site sought and received approval from the relevant local research ethics  
484 committee. Written consent was obtained from each participant and a parent or  
485 guardian.

486 **Munich-Depression**

487 The studies were approved by the respective local ethics committees: The ethical  
488 committee of the Ludwig-Maximilians-Universität, Munich, Germany and the ethical  
489 committee of the Bayerische Landesärztekammer, Munich, Germany. All participants  
490 provided written informed consent.

491 **TOP**

492 All participants were recruited between 2003 and 2009 as part of an ongoing study of  
493 psychotic disorders (Thematically Organized Psychosis study). After complete  
494 description of the study, all participants gave informed consent to participate. The

495 study was approved by the Regional Committee for Medical Research Ethics and the  
496 Norwegian Data Inspectorate.

497 **ADHD**

498 This study was approved by the regional ethics committee (Centrale Commissie  
499 Mensgebonden Onderzoek: CMO Regio Arnhem – Nijmegen; 2008/163; ABR:  
500 NL23894.091.08) and the medical ethical committee of the VU University Medical  
501 Center. Informed written consent was obtained from each participant. For children  
502 under 18, both parents and children gave consent.

503 **Study Protocol**

504 We developed a method, termed msCCA-regression to find multivariate relationships  
505 between psychiatric symptoms, and multiple neuroimaging modalities  
506 simultaneously; In this case, voxel-based morphometry (VBM)<sup>18</sup> measures of grey  
507 matter volume, fractional anisotropy (FA) derived from DTI data, and normalized  
508 using tract based spatial statistics (TBSS)<sup>19</sup>, and resting state functional connectivity  
509 neuroimaging measures<sup>43</sup>. msCCA-regression analysis was carried out in the  
510 general population IMAGEN sample, when participants were aged 19. Additional  
511 analyses were then applied in order to localize associations between psychiatric  
512 symptoms, and neuroimaging measures of brain structure and function. We then  
513 analyzed neuroimaging and symptom data at age 14 in order to determine whether  
514 this multivariate relationship already existed at this earlier time-point. Following this,  
515 we assessed the clinical significance of our findings by conducting case-control  
516 comparisons of the structural markers found in the IMAGEN analysis, in several  
517 clinical samples. The following text gives a more detailed description of the methods  
518 described here.

## 519 **IMAGEN Analysis**

520 IMAGEN is a large-scale neuroimaging-genetics cohort study conducted with the aim  
521 of understanding the biological basis of individual variability in psychological and  
522 behavioural traits, and their relation to common psychiatric disorders<sup>44</sup>. The study  
523 involves a thorough neuropsychological, behavioural, clinical and environmental  
524 assessment of each participant. Participants also undergo biological  
525 characterisation, with the collection of T<sub>1</sub> weighted MRI (sMRI), diffusion tensor  
526 imaging (DTI), task-based fMRI (t-fMRI), resting-state fMRI (rs-fcMRI) and genetic  
527 data. We used T<sub>1</sub> weighted, DTI, and rs-fcMRI data in the current investigation.

## 528 **Participants**

529 The analysis was carried out on participants drawn from the IMAGEN sample (see  
530 for further details: Schumann et al<sup>44</sup>. For IMAGEN, a general population sample of  
531 Caucasian adolescents were recruited from eight sites across France, Ireland,  
532 England and Germany. Data was collected at age 14, 16 and 19 years. After a  
533 conservative quality control of MRI acquisitions and DAWBA questionnaires,  
534 participants with complete data were used in the subsequent data analysis. No  
535 statistical analyses were used to pre-define sample size. However, the sample size  
536 used was similar to that reported in previous studies<sup>10,12</sup>.

## 537 **DAWBA**

538 Psychiatric symptoms of the IMAGEN participants were assessed using screening  
539 questions from the development and wellbeing assessment (DAWBA), a wide  
540 ranging psychiatric screening questionnaire<sup>45</sup>. Participants were asked screening  
541 questions, assessing symptoms of: specific fears, social fears, stress after a very

542 frightening event, obsessions and compulsions, worrying, depression, rapidly  
543 changing mood, attention and activity, troublesome behavior, drug and alcohol use,  
544 concern about appearance and strange/frightening experiences; if enough of these  
545 questions were answered in the affirmative, a more in-depth assessment of  
546 symptoms associated with that disorder was made. DAWBA screening questions  
547 have previously been used to define subthreshold clinical symptoms in neuroimaging  
548 studies of subclinical psychopathology<sup>46</sup>. The strength and difficulties questionnaire  
549 (SDQ) was also used in the present investigation as this questionnaire contributes to  
550 the assignment of diagnostic status in the DAWBA<sup>45</sup>. Questions in the SDQ are  
551 categorized into broad internalising and externalizing domains. The data of four of  
552 the questions asked had a standard deviation of zero amongst the participants  
553 asked, and were therefore not used in subsequent analyses. The full set of  
554 psychiatric questions asked in the present investigation can be found in  
555 Supplementary Table 1, the questionnaire items that were omitted from the analysis  
556 are marked here. At the time of the analysis conducted here, DAWBA/SDQ data had  
557 been collected for 1510 participants. Of these, data was incomplete for 239  
558 participants, and was not used.

559

#### 560 **T<sub>1</sub> Weighted MRI Acquisition**

561 Scanning took place at eight different sites across Europe, using scanners built by  
562 four different manufacturers (Siemens, Philips, General Electric, Bruker). High  
563 resolution, T<sub>1</sub> weighted images were obtained using a Magnetization Prepared Rapid  
564 Acquisition Gradient Echo (MPRAGE) sequence, based on the ADNI protocol  
565 (<http://www.loni.ucla.edu/ADNI/Cores/index.shtml>). Scan parameters were  
566 standardized across sites to the highest degree possible (sagittal slice plane;

567 repetition time: 2.3 s; echo time 2.8 ms; flip angle 8°; 256×256×160 matrix; isotropic  
568 voxel size: 1.1 mm).

### 569 **VBM Pre-processing**

570 At the time this investigation was conducted, T<sub>1</sub> data had been acquired for 1400  
571 participants. All scans were visually inspected and manually reoriented. 285 scans  
572 were discarded from the analysis for either movement artifacts, strong field  
573 inhomogeneities, abnormal field of view, abnormally reduced cerebellum and for  
574 brace artefacts. The resulting 1,115 scans were used to build the study specific  
575 template. Baseline and Follow up two scans were preprocessed using both the 2008  
576 version of the Voxel Based Morphometry toolbox (VBM8) running in SPM8 (v.5236).  
577 Given the young adults recruited in IMAGEN, we first used VBM8 in order to avoid  
578 using adult tissue probability maps (TPM) to initiate the segmentation process. The  
579 VBM8 toolbox segmentation relies on an adaptive Maximum a Posterior technique  
580 and TPMs used in VBM8 are for registration purposes only. Diffeomorphic  
581 registration (Dartel) was then used to register the 1,115 images, and to generate the  
582 study-specific population average template<sup>47</sup>. We then resliced the data to  
583 1.5x1.5x1.5mm voxel size. Smoothing was carried out using an isotropic 8 mm full  
584 width at half maximum Gaussian smoothing kernel. We created a mask for the  
585 sample by taking the mean across all VBM maps included in the sample. We  
586 thresholded the mask at >0.4. We used a stringent mask to avoid overfitting the  
587 data<sup>48</sup>. We then extracted all voxel values within this mask, resulting in 241,544 grey  
588 matter voxels.

### 589 **DTI Acquisition**

590 Diffusion tensor imaging acquisition sequence based on the study by Jones et  
591 al<sup>49</sup>. Diffusion tensor images were acquired using an Echo Planar imaging sequence  
592 ( $b=0$  and 32 directions with  $b$ -value  $1300 \text{ s/mm}^2$ ; axial slice plane; echo time =  
593  $104 \text{ ms}$ ;  $128 \times 128 \times 60$  matrix; voxel size  $2.4 \times 2.4 \times 2.4 \text{ mm}$ ), adapted to tensor  
594 measurements (for example, FA, mean diffusivity (MD)) and tractography analysis.

595

### 596 **TBSS Pre-processing**

597 At the time this study was conducted, DTI data had been acquired for 1412  
598 participants. Of these, 71 were not usable due to: signal dropouts or too much  
599 rotation. Diffusion imaging data was pre-processed using software from the FSL  
600 toolbox ([www.fmrib.ox.ac.uk/fsl](http://www.fmrib.ox.ac.uk/fsl))<sup>50</sup>. We preprocessed the remaining 1341 scans  
601 using tract based spatial statistics (TBSS)<sup>19</sup>. Pre-processing was carried out in the  
602 following manner: An affine registration was applied to the first  $B_0$  image for head  
603 motion and eddy current correction. Brain extraction was carried out using BET.  
604 Diffusion tensor fitting was then used to obtain fractional anisotropy (FA) maps for  
605 each participant. All participants' FA data was aligned into a common space using  
606 the non-linear registration tool FNIRT, using a b-spline representation of the  
607 registration warp field. The mean was then taken across all FA maps to create an FA  
608 averaged image. This map was then 'thinned' to create a mean FA skeleton, which  
609 was then thresholded at  $FA > 0.2$ , keeping only the major white matter tracts. Each  
610 participant's aligned FA data was then projected onto the mean skeleton. We then  
611 used these skeletonised maps in all subsequent analyses. The final mask used  
612 contained 106,812 voxels. A further 10 scans were not used due to masking or  
613 normalization issues in TBSS.



## 614 **Resting State fMRI Acquisition**

615 Resting state fMRI scanning of the IMAGEN participants was carried out at multiple  
616 sites. The following parameters were standardized: number of volumes (164), TR =  
617 2.2s, TE = 30ms, flip angle = 75, number of slices/ddas = 40/3, slice thickness = 2.4  
618 mm, slice gap = 3.4 mm, voxel size = 3.4 x 3.4 x 2.4 mm<sup>3</sup>, matrix size = 64<sup>2</sup>, FOV =  
619 218 mm.

## 620 **Resting State fMRI Preprocessing**

621 At the time of this investigation, we had collected rsfMRI scans for 1067 participants.  
622 Of these scans, 157 were not used, either because over 5% of scans in that  
623 participant exhibited artifacts of some kind, or if over 5% of volumes showed a  
624 fractional displacement of over 0.5mm. Preprocessing of resting-state data was  
625 performed with routines from FMRIB's Software Library (FSL v5.0.9)<sup>50</sup> and Advanced  
626 Normalization Tools (ANTs v1.9.2)<sup>51</sup>.

- 627 1) Motion correction was carried out, applying a rigid body registration of each  
628 volume to the middle volume (FSL MCFLIRT).
- 629 2) Non-brain tissue was removed (FSL BET).
- 630 3) Spatial smoothing was applied using a 5mm FWHM Gaussian kernel.
- 631 4) Independent component analysis (FSL MELODIC) was run for each data set.  
632 Artifact components were identified using an automatic classification  
633 algorithm, and subsequently regressed from the data (ICA-AROMA v0.3)<sup>52,53</sup>.  
634 ICA-AROMA<sup>52</sup> has been shown to be as effective as motion parameter  
635 regression, with additional spike regression and 'scrubbing', in the removal of

636 motion related effects on functional connectivity measures derived from  
637 resting state fMRI data. However, this procedure has the additional benefit  
638 that it preserves more signal of interest than these methods<sup>53</sup>.

639 5) The resulting cleaned data set was de-trended (up to a third degree  
640 polynomial).

641 6) Co-registration to a high-resolution T<sub>1</sub> image (FSL FLIRT using the BBR  
642 algorithm), and normalization to 2mm isotropic MNI standard space (ANTs)  
643 was carried out.

644 7) We used the CompCorr procedure to further clean the data of physiological  
645 noise<sup>54</sup>. To do this: we created white matter (WM) and cerebrospinal fluid  
646 (CSF) masks by taking the mean of the WM and CSF segmentations from the  
647 VBM analysis, and thresholding them at 0.95, we then resliced these maps  
648 into the same space as the rsfMRI data. We then extracted timecourses from  
649 voxels within these regions, and took the first three principal components of  
650 this signal for both WM and CSF maps. These six principal component signals  
651 should represent non-neuronal signal. We then regressed this non-neuronal  
652 signal from voxel timecourses across the rest of the brain.

653 8) Lastly, preprocessed and normalized resting-state data sets were resliced to  
654 3mm isotropic voxels.

655

656

657 **Mapping rs-fMRI data**

658 1) We first generated 55 regional nodal timecourses using dual regression on  
659 nodal regions established in the UK biobank sample<sup>17</sup>.

660 2) We mapped the correlation between nodal regions using Pearson's pairwise  
661 correlation coefficient, for each participant, thus producing a connectivity  
662 matrix for each participant. This connectivity matrix consists of 1,485  
663 connections between nodes.

664 3) We then transformed these connectivity values using Fisher's Z-score  
665 transform.

### 666 **Different Neuroimaging Processing Strategies**

667 A wide range of different preprocessing strategies can be applied in the analysis of  
668 neuroimaging data. Approaches to analysing DTI and T1 can be categorised into two  
669 broad types: voxelwise, and atlas based approaches<sup>18,55</sup>. We chose to analyse this  
670 data at the voxelwise level, as this allows for the highest level of spatial specificity.  
671 Although it is also technically possible to analyse rs-fcMRI data across the whole  
672 brain at the voxelwise level, this approach results in an enormous number of  
673 features: When mapping connectivity at the voxelwise level, in a dataset made up of  
674  $N$  voxels, we are left with  $(N*(N-1))/2$  connections between those voxels. In the  
675 current investigation,  $N = 57,053$ , leading to  $N*(N-1)/2 = 1.63$  billion inter-regional  
676 connections. This would lead to a huge amount of redundancy in the data and  
677 computational, statistical and interpretational issues. For this reason, we mapped the  
678 connectivity between a pre-defined set of nodes. We used nodal definitions resulting  
679 from previous work applying independent component analysis (ICA) to the UK  
680 biobank sample<sup>17</sup>. We used this nodal definition as it derives from the largest extant  
681 sample of neuroimaging data. In order to test whether the results we obtained were

682 robust to different nodal definitions, we also mapped inter-regional connectivity using  
683 the widely used Power atlas<sup>56</sup> and achieved similar results (Supplementary Figure  
684 6).

### 685 **Canonical Correlation Analysis and Sparse Canonical Correlation Analysis**

686 Canonical correlation analysis (CCA) is a very general statistical method used to  
687 identify linear relationships between two or more sets of variables<sup>57</sup>. It can be  
688 thought of as a generalization of multiple linear regression. The objective of CCA is  
689 to identify a relationship between two (or more) sets of variables, where there is no  
690 distinction between which variables are considered dependent, and which are  
691 considered independent. This method identifies weights for each variable, such that  
692 the weighted sum of variables in each set is maximally correlated with the weighted  
693 sum of variables from the opposite set, assuming a linear relationship.

694 Consider two matrices  $X_1$  and  $X_2$ , where each row denotes one of  $n$  observations,  
695 and each column denotes one of  $p_1$  or  $p_2$  features. CCA seeks to find the weight  
696 vectors  $w_1$  and  $w_2$  that maximise the correlation:

$$697 \quad \rho = \text{corr}(X_1 w_1, X_2 w_2).$$

698 This optimisation problem can be written as:

$$\rho = \max_{w_1, w_2} w_1^T X_1^T X_2 w_2$$

699 Subject to the constraints:

$$700 \quad w_1^T X_1^T X_1 w_1 = 1 \text{ and } w_2^T X_2^T X_2 w_2 = 1.$$

701 We assume that the columns of  $X_1$  and  $X_2$  have been standardised to have a mean of  
702 zero and a standard deviation of one. The vectors  $X_1 w_1$  and  $X_2 w_2$  are referred to as  
703 canonical variates.

704 Classical CCA is extremely powerful, but cannot be applied in situations where there  
705 are a more features than samples (i.e.,  $p_1 > n$  or  $p_2 > n$ , which is typically the case in  
706 neuroimaging studies). Interpreting and describing results from CCA can be difficult  
707 because the estimated weights are not sparse. This means that some variables may  
708 make negligible but non-zero contributions to the variance explained between sets.  
709 Sparse canonical correlation analysis (sCCA) was developed to address these  
710 issues<sup>11,58,59</sup>.

711 sCCA uses an  $L_1$  penalty on canonical weights, which forces some of them to take a  
712 value of exactly zero. Furthermore, sCCA can also be applied in scenarios where  
713 there are more features than samples ( $p > n$ ). The optimization criteria for sCCA can  
714 be written in the following manner:

$$\rho = \max_{w_1, w_2} w_1^T X_1^T X_2 w_2$$

715 Subject to the constraints:

716  $\|w_1\|^2 = 1, \|w_2\|^2 = 1, \|w_1\|_1 \leq c_1$  and  $\|w_2\|_1 \leq c_2$

717 Here,  $c_1$  and  $c_2$  are assumed to fall within the bounds  $1 \leq c_1 \leq \sqrt{p_1}$  and  $1 \leq c_2 \leq \sqrt{p_2}$ ,  
718 where  $p_1$  and  $p_2$  are the number of features in views  $X_1$  and  $X_2$  respectively.

### 719 **Multiple Sparse Canonical Correlation Analysis Regression**

720 The formulation of sparse canonical correlation analysis described in the text above  
721 is designed to find relations between two views of a dataset. However, we have

722 collected data from several different neuroimaging modalities, and would like to  
723 utilize information from each of them. A somewhat naive approach to finding  
724 relations between psychiatric symptoms and multiple neuroimaging measures would  
725 be to include all available neuroimaging modalities in one view of the canonical  
726 relation, with psychiatric symptoms in the other view. However, this approach is likely  
727 to be problematic as different modalities are associated with very different numbers  
728 of features. For example, the functional connectivity data used in the present  
729 investigation has only 0.6% of the number of features that the VBM data has. As  
730 such, if these modalities were entered into the same model, the VBM data would  
731 overwhelm the functional connectivity data.

732 We developed an approach designed to maximise the cross-correlation between  
733 psychiatric symptoms, and multiple neuroimaging modalities simultaneously, we then  
734 combined these modalities in a linear regression model. Formulations of canonical  
735 correlation analysis that are able to find relations between more than two sets of data  
736 are termed multiple or generalised canonical correlation procedures. A widely used  
737 optimisation criteria for multiple canonical correlation analysis is to maximise the sum  
738 of correlations between each of the different views of a dataset<sup>60</sup>. Witten et al have  
739 formulated a sparse version of multiple canonical correlation analysis<sup>58</sup>; this  
740 formulation is designed to maximise the sum of correlations between all views of the  
741 data. However, in the present investigation, we are only interested in finding  
742 correlations between neuroimaging measures, and psychiatric questionnaire  
743 responses; we do not wish to optimise the correlation between different  
744 neuroimaging measures.

745 As such, we seek to maximise the following relation:

$$\max_{w_1, \dots, w_n} w_1^T X_1^T \sum_{i=2}^n X_i w_i$$

746 Subject to the constraints:

747  $\|w_1\|^2 = 1, \|w_i\|^2 = 1, \|w_1\|_1 \leq c_1$  and  $\|w_i\|_1 \leq c_i$

748 This method simultaneously optimizes the correlation between a weighted sum of  
749 variables in the target set,  $X_1$ , with a weighted sum of variables in the other sets. In  
750 the present investigation,  $X_1$  is a matrix of psychiatric symptoms and  $X_2$  to  $X_n$  are  
751 neuroimaging measures of brain structure and function. Using this method, we are  
752 able to maximise the correlation between psychiatric symptoms, and several  
753 different neuroimaging modalities within the same integrated model. A natural choice  
754 for the statistic of interest, in any inference carried out using this procedure, would be  
755 the sum of correlations between the symptom data, and the neuroimaging measures  
756 of brain structure and function. However, a sum of correlations is of less practical  
757 benefit than understanding how much total variance is shared between  
758 neuroimaging measures of brain structure and function, and psychiatric symptoms.  
759 Therefore, in the final step of this process, we combine canonical neuroimaging  
760 variables in an ordinary linear regression model. Canonical variables are defined as:

$$C_i = X_i w_i$$

761 Canonical variables are then combined in the prediction of psychiatric symptoms  
762 using ordinary linear regression:

$$C_1 = \beta_0 + C_2\beta_2 \dots + C_n\beta_n + \epsilon$$

763 We used this approach to establish relations between psychiatric symptoms ( $C_1$ ),  
764 and TBSS ( $C_2$ ), VBM ( $C_3$ ), and connectivity measures ( $C_4$ ) derived from rs-fMRI data  
765 and  $\beta_n$  are the associated weights estimated using ordinary linear regression ( $\beta_0$  is  
766 the constant estimated in regression).

767 msCCA-regression was carried out using in-house codes written in MATLAB. This  
768 algorithm requires an initialization value. In the present study, initial weights were  
769 randomly generated. Weight values associated with psychiatric symptoms were  
770 always constrained to be positive to ensure interpretability.

771 This study is designed to be exploratory in nature. Nevertheless, given the very large  
772 quantity of data we sought to integrate, it is likely that some simple priors will help to  
773 improve the stability of our results, so long as those priors are well supported. There  
774 is a great deal of evidence suggesting that psychopathology is associated with  
775 decreases in both grey matter, and fractional anisotropy, across psychiatric  
776 disorders<sup>61,62</sup>. For this reason, we constrained the canonical weights on VBM volume  
777 and FA to be negative. This will help to reduce variance in the model and will help  
778 increase interpretability of our results. In contrast, there is no clear evidence that  
779 psychiatric illness is associated with increases or decreases in connectivity  
780 measures derived from BOLD-fMRI. Therefore, we did not add constraints to the  
781 functional connectivity data.

782



## 783 **Stability Selection**

784 Although msCCA-regression (and sCCA) have advantages over classical CCA in  
785 terms of interpretability, it can suffer from instabilities due to their utilization of an  $L_1$   
786 penalty to introduce sparsity<sup>21</sup>. This is particularly true when  $p \gg n$ , and when there  
787 is a high degree of collinearity in the data. Stability selection is a widely applicable  
788 feature selection procedure that can address this problem<sup>21</sup>. This procedure has the  
789 added benefit that it makes the results less sensitive to the choice of  $L_1$  penalty.

790 The conceptual underpinning of stability selection is very simple: if a model is  
791 repeatedly resampled, features exhibiting a 'real' effect will be selected more often  
792 than noise. Using stability selection, data is repeatedly split into random sub-samples  
793 of size  $n_t/2$  (where  $n_t$  is the total number of participants in the training dataset). In this  
794 work, resampling was carried out a hundred times. msCCA was applied to each  
795 resample, and those features that appear more often are deemed to be more stable.  
796 Deciding which variables are stable requires a threshold:  $\pi_r$  is defined as the fraction  
797 of samples in which a particular variable must be observed to be considered stable.  
798 We set  $\pi_r$  to 0.9, which means that a particular variable must be present in 90% of  
799 resamples to be considered stable. The outcome of this stability selection procedure  
800 is a set of stable features. A benefit of stability selection is that it is insensitive to  
801 tuning parameters. Here, we simply set the  $L_1$  penalty at  $\sqrt{p}/2$ , which is halfway  
802 along the regularization path running from 1 to  $\sqrt{p}$ . It is worth noting that the stability  
803 selection procedure is easily parallelizable here as it simply involves re-applying the  
804 msCCA-regression algorithm to multiple different resamples of the same data.

805

## 806 **Analysis Design**

807 The  $L_1$  penalty used in sCCA means that the parametric tests used for significance  
808 testing in classical CCA (for example Wilk's Lambda)<sup>63</sup> cannot be used here,  
809 necessitating the use of permutation testing to determine whether results are  
810 significant. We assessed the in-sample significance of the results we obtained here,  
811 then replicated these findings using an out-of-sample, hold-out set design. This kind  
812 of experimental design has a number of advantages in the present context: using a  
813 training/testing design, it is possible to obtain an unbiased estimate of effect size. We  
814 used a hold-out set design in preference to a cross-validation procedure. This is  
815 because cross-validation involves the training and testing of multiple statistical  
816 models, one for each cross-validation fold, which precludes the use of a single model  
817 for further validation/characterization. A related advantage is that it is possible to  
818 carry out further characterization of the test set results, due to the fact that we are  
819 able to estimate effect size in an unbiased way.

820 In detail, the analysis design was carried out as follows:

- 821 1) Psychiatric symptom data, and data from the VBM, TBSS and rs-fcMRI  
822 neuroimaging modalities was extracted and transformed into  $n_t \times p_i$  matrices,  
823 where  $n_t$  is the number of participants included in the training dataset, and  $p_i$   
824 is the number of features included in each of the views of the data.
- 825 2) The full dataset was randomly split into training and testing sets. The training  
826 set was made up of 70% of the data whilst the testing set was made up of the  
827 remaining 30%.

828 3) The training data was then randomly split into a hundred further resamples.  
829 Each resample was made up of  $n_t/2$  participant scans, where  $n_t$  is the total  
830 number of participants in the training dataset.

831 4) The first stage of the mSCCA- regression algorithm (see above) was then  
832 applied to each resample, with a sparsity constraint of  $\sqrt{p_i}/2$  in each view of  
833 the data.

834 5) We then recorded which variables, in each view of the data, are present in  
835 over 90% of resamples. These variables are considered to be stable, and are  
836 retained.

837 6) We then re-applied the msCCA algorithm to the data, without sparsity  
838 constraints, on the variables that survived more than 90% of resamples.

839 7) We then combined the neuroimaging canonical variates we found in the  
840 previous step in a prediction model on the symptom canonical variate, using  
841 ordinary least squares regression. We then recorded the correlation between  
842 the neuroimaging prediction model, and the symptom canonical correlate.

843 8) We then permuted the training data, and repeated steps 3-7. This was done  
844 for 10,000 different permutations of the training data labelling. In each case,  
845 we recorded the correlation between the neuroimaging model, and the  
846 canonical correlate of psychiatric symptoms. In this way, we built up a  
847 permutation distribution to assess the significance of the relation between  
848 symptom and neuroimaging data in the experimental labelling, within the  
849 training dataset.

850 9) We then applied the trained model to the test set to produce canonical  
851 correlates of symptom and neuroimaging measures. We recorded  
852 associations for both the full model, and between the psychiatric symptom  
853 score, and each of the individual neuroimaging canonical correlates.

854 10) We then randomly permuted the data rows in the testing set and re-  
855 calculated correlation values between symptom and brain canonical  
856 correlates. We recorded associations between psychiatric symptoms and the  
857 full neuroimaging model, for each of 10,000 permutations of the experimental  
858 labelling.

859 11) It is also interesting to find the significance of the individual neuroimaging  
860 modalities. However, as we are testing the significance of multiple  
861 neuroimaging modalities, it is necessary to correct for multiple comparisons  
862 across these different modalities. This is easily done using the distribution of  
863 the maximal statistic: for each permutation of the experimental labelling, we  
864 calculate the association between the symptom score and each of the  
865 neuroimaging canonical correlates; the largest of these associations is then  
866 recorded. This is done for each of the 10,000 permutations of the test  
867 labelling, producing a distribution of the maximal statistic. Correlations  
868 between symptom and neuroimaging measures in the experimental labelling  
869 are then significant at the FWE-corrected level  $\alpha$  if they are above the  $100*(1-$   
870  $\alpha)$  percentile of this distribution.

871 This process is illustrated in Supplementary Figure 1.

872

873 **Confounds**

874 It is important to account for the effects of confounds, which might otherwise lead to  
875 spurious relations between the different data views<sup>64</sup>. Here, we regressed age,  
876 gender, site and intracranial volume from all data views prior to the sCCA analysis<sup>65-</sup>  
877 <sup>67</sup>. For the connectivity measures derived from rsfMRI data, we also regressed the  
878 mean between-volume fractional displacement, and the percent of slices corrupted  
879 by artefacts, from the scans.

880 **Additional Analyses to Localise Effects**

881 We used msCCA-regression to find multivariate relations between psychiatric  
882 symptomatology and neuroimaging measures of brain structure and function. In  
883 using msCCA-regression, it is possible to make inferences on relations between sets  
884 of psychiatric symptoms and neuroimaging measures across the brain, it is not  
885 possible to make inferences on individual brain regions/connections or individual  
886 questionnaire items. For this reason, we conducted additional analyses to further  
887 deconstruct the relationship between psychiatric symptomatology and the brain. This  
888 procedure is similar to a redundancy analysis<sup>68,69</sup>. In particular, we were interested in  
889 localising which brain regions exhibited an individually significant association with  
890 psychiatric symptomatology.

891 Conducting further tests on the whole dataset would introduce circularity into the  
892 analysis. Therefore, additional inference must be carried out on the testing dataset  
893 alone. Nevertheless, the training dataset is still likely to contain useful information,  
894 which can be used to guide analyses carried out on the testing dataset, thus  
895 decreasing the multiple comparison problem, and increasing the likelihood of finding  
896 significant effects in the testing dataset. In the present investigation, we looked for

897 significant localizable effects in the training dataset, we then used these results to  
898 inform analyses carried out on the testing dataset. In this sense, the training dataset  
899 was used as a 'discovery dataset'.

900 In the case of the TBSS and VBM data, we sought to localize associations between  
901 symptoms and the brain to the cluster-wise level. In the case of the rs-fcMRI data,  
902 we sought to localize changes to individual inter-regional connections. VBM and  
903 TBSS clusters were defined using an 18-connectivity scheme. This means that  
904 voxels must be connected by a face or an edge to be considered a part of the same  
905 cluster.

906 This analysis was carried out in the manner described below:

- 907 1) We calculated the grey matter volume and FA in spatially distinct clusters  
908 identified in the sCCA analysis applied to VBM and TBSS respectively. We  
909 extracted connectivity values with non-zero canonical weights. This was done  
910 in both the training and testing datasets.
- 911 2) We calculated Pearson's correlation coefficient between the mean of each  
912 spatially distinct cluster/connection, and the sum of symptom score values.  
913 This was done separately in the training and testing datasets.
- 914 3) Rows associated with neuroimaging data in the training set were permuted  
915 and correlations between clusters/connections, and symptom clusters were  
916 recalculated. The maximal value was recorded. Training data was permuted  
917 10,000 times; the maximum correlation value across all clusters/connections  
918 was recorded for each permutation. Clusters/connections exhibiting a  
919 significant effect in the training dataset were then determined by comparing

920 correlation values to the distribution of the maximal statistic<sup>50, 51</sup>. Because  
921 model selection was carried out in the training dataset, conducting inference  
922 on the training dataset would constitute “double dipping”.

923 4) Clusters/connections exhibiting a significant effect in the training dataset were  
924 taken forward for an analysis carried out in the testing set.

925 5) We calculated correlation values between clusters/connections in the testing  
926 dataset, and the symptom score.

927 6) Testing data was permuted 10,000 times; the maximum correlation value  
928 across all clusters/connections was recorded for each permutation.

929 Clusters/connections exhibiting a significant effect in the testing dataset were  
930 determined by comparing correlation values to the distribution of the maximal  
931 statistic. Cluster/connection correlations in the testing dataset were then  
932 compared to correlations in the distribution of the maximal statistic.

933 Cluster/connection correlations in the experimental labelling, which were in  
934 the top 5% of the distribution of the maximal statistic, were considered  
935 significant at the FWE corrected level.

936 This process is illustrated in Supplementary Figure 3.

### 937 **Finding Multiple Modes of Variation**

938 Using canonical correlation analysis, it is possible to uncover multiple modes of  
939 variation between datasets. After determining the significance of the first canonical  
940 correlate, we remove the effect of the first set of canonical vectors, and repeat the  
941 analysis. Witten et al used Hotelling's deflation to remove the effect of the first vector;  
942 this approach has been criticized by Monteiro et al, who propose the projection

943 deflation procedure as an alternative<sup>11,70</sup>; this is the procedure we use in the present  
944 investigation. Correlations between the different canonical relations are given in  
945 Supplementary Table 6.

946 It is possible to ascertain the significance of all canonical relations after the first by  
947 comparing the correlations of subsequent associations to the permutation distribution  
948 of the first relation: The first canonical relation between sets is by definition the  
949 strongest; any subsequent associations between sets will be weaker than the  
950 canonical relation that preceded it. A common means of correcting for multiple  
951 comparisons is to compare test statistics in the experimental labelling to the maximal  
952 statistic across all tests in the permutation distribution; this distribution is usually  
953 termed the distribution of the maximal statistic<sup>71,72</sup>. In the present investigation, we  
954 can find this distribution by recording the strength of the first canonical relation, for  
955 each permutation. Significance values that are corrected for multiple comparisons  
956 can then be found by comparing associations of subsequent modes of variation, with  
957 this distribution<sup>73</sup>.

### 958 **Hypothesis Driven Analysis**

959 A major advantage of the approach described here is that it allows the grouping of  
960 psychiatric illnesses to be driven by their biological underpinnings. Nevertheless, it is  
961 an open question whether the symptom groups discovered in the data driven  
962 analysis we ran here show a stronger relation to neuroimaging measures of brain  
963 structure and function than pre-defined symptom groups. For this reason, we tested  
964 whether the widely used internalising/externalising organisation of psychiatric illness  
965 is able to explain as much variance in psychiatric symptomatology as this purely data  
966 driven method. To do this, we used an approach that is as similar as possible to the



967 primary data analysis followed in the main part of the investigation, yet still makes  
968 use of the internalising/externalising illness structure: we replaced the symptom  
969 matrices used in the main part of the investigation with symptom vectors based on  
970 previously defined internalising and externalizing symptom sub-scales from the  
971 DAWBA; no sparsity was applied to psychiatric symptom sub-scales. Used in this  
972 manner, the msCCA-algorithm reduces to something like a sparse partial least  
973 squares regression<sup>74</sup>, where the neuroimaging features are predictors and the pre-  
974 defined internalising/externalising vectors are the targets. This method was applied  
975 twice, once to predict the internalising symptom dimension, and once to predict the  
976 externalising. We term the internalizing and externalising symptom scales as  
977 DAWBA-internalising and DAWBA-externalising respectively. We defined symptoms  
978 as belonging to broad internalising or externalising categories in the same way as  
979 Aebi et al<sup>75</sup> : The DAWBA-internalising scale was created by summing: specific  
980 fears, social fears, panic attacks, stress after a frightening event, worrying and  
981 depression. The DAWBA-externalising scale was created by summing: Attention and  
982 activity, behaviours and attitudes that can get people into trouble, and Cigarettes,  
983 Alcohol and Drugs sections of the DAWBA. The SDQ is already split into broad  
984 internalising and externalising domains<sup>45</sup>. Therefore, internalising and externalising  
985 SDQ scores were simply added to these scores to create DAWBA-internalising and  
986 DAWBA-externalising scores respectively. The sections: rapidly changing mood,  
987 dieting and bingeing and strange experiences that are surprisingly common were not  
988 used to create scores as these symptoms do not fit neatly into an  
989 internalising/externalising dichotomy. All of these questions can be found in  
990 Supplementary Table 1.

991

992 **Longitudinal Analysis**

993 The msCCA-regression analysis described above was used to find relations between  
994 psychiatric symptoms and neuroimaging measures of brain structure at age 19,  
995 when participants were young adults. However, the developmental time period  
996 immediately preceding this time point is also of potential interest, with the brain going  
997 through important maturational processes and participants being at increased risk for  
998 the development of psychopathology<sup>76</sup>. Thus, we applied the msCCA-regression  
999 algorithm between psychiatric symptoms and neuroimaging measures at age 14.  
1000 The results of this analysis are show in Supplementary Figure 8. We did not find a  
1001 significant relation between psychiatric symptoms and the brain at this age. As rs-  
1002 fMRI data is only available for a small sub-sample of the full dataset at age 14, we  
1003 only used VBM and TBSS data in this analysis.

1004 It is possible that neuroimaging markers of psychiatric illness precede the  
1005 development of full-blown psychiatric symptomatology. To determine whether this  
1006 was the case in the present investigation, we took the TBSS and VBM regions  
1007 identified as being associated with psychopathology at age 19, we then extracted the  
1008 appropriate neuroimaging data from these brain regions at age 14, and correlated  
1009 the output with symptoms at age 19. In this way, we showed that neuroimaging  
1010 measures at age 14 have predictive value for psychopathology at age 19.

1011 For these analyses, we used the same subjects as were included in our  
1012 analysis at age 19. We also used the same train-test split within this subject group.  
1013 We subjected this age 14 data to the same QC procedures as the data taken at age  
1014 19. Of the n = 666 subjects used in the msCCA-regression analysis carried out at  
1015 age 19, 72 subjects had data that did not pass QC at age 14. This left n = 594

1016 subjects for age 14 analyses, with  $n = 412$  subjects in the training group and  $n = 182$   
1017 in the testing/replication group.

### 1018 **Clinical Analyses**

1019 Using mSCCA-regression, we found a set of neuroimaging features that correlate  
1020 with a set of questions assessing psychiatric health. At the group level, participants  
1021 who score more highly on the vector derived from neuroimaging data will suffer a  
1022 larger number of psychiatric symptoms (as measured by the DAWBA). It might  
1023 therefore be expected that participants with a clinical diagnosis of a psychiatric  
1024 disorder would score more highly on this neuroimaging vector than healthy controls.  
1025 To discover whether this was the case, we subjected clinical data to exactly the  
1026 same pre-processing as the IMAGEN data; we then looked for changes in grey  
1027 matter volume in the regions identified in the initial analysis. A (one-sided) two-  
1028 sample t-test was used to determine whether patients and controls differed  
1029 significantly on this one-dimensional measure. We only used grey matter data here  
1030 as this data-type showed the strongest relation to psychopathology in the IMAGEN  
1031 sample. Furthermore, this data-type is widely available and the number of degrees of  
1032 freedom in the MRI scan acquisition parameters is low. The case-control tests we  
1033 used here make the assumption of data normality, although this was not formally  
1034 tested here.

1035 We used the same confounds in this analysis as we did on the IMAGEN data, this  
1036 includes the use of total grey matter as a covariate of no interest. However, it could  
1037 still be argued that regional changes are only acting as a proxy for total grey matter.  
1038 In order to determine whether this is the case, we repeated all pertinent analyses,

1039 using total grey matter as a regressor in addition to total intracranial volume. The  
1040 results of these analyses are shown in Supplementary Figure 10.

1041

#### 1042 **Depression sample**

1043 The Munich sample consisted of patients with first episode and recurrent unipolar  
1044 Depression treated as in-patients at the Max Planck Institute of Psychiatry, Munich,  
1045 and healthy control participants. The data for 13 of the participants assessed was not  
1046 used as it was deemed to be of insufficient quality, this left: N=614; 400 patients, age  
1047 48 [SD 13.8] years, 53% women; 214 control participants age 49 [SD 13.3] years,  
1048 58% women, for the most part overlapping with imaging genetic and MDD  
1049 association studies reported in collaboration with the ENIGMA consortium<sup>22,77</sup>. Other  
1050 than in the two flagship studies, no bipolar patients were included for reasons of  
1051 clinical homogeneity. MDD diagnoses were based on clinical consensus in addition  
1052 to M-CIDI or SCAN interviews, depending on the original study protocols. The  
1053 Munich sample comprised images acquired in subsamples of the Munich  
1054 Antidepressant Response Signature Study and the Recurrent Unipolar Depression  
1055 Case-Control study, both performed at the MPIP. We did not use any statistical  
1056 analyses to decide on the sample size used here. However, the sample used was  
1057 among the largest of any single study investigating alterations in brain structure in  
1058 depressed participants<sup>77</sup>.

#### 1059 **Schizophrenia/Bipolar sample**

1060 Participants with schizophrenia and bipolar disorder were recruited from the  
1061 Thematically Organised Psychosis (TOP) study. This is a collaborative study based  
1062 at the University of Oslo in Norway. The data for 2 participants was not used as it

1063 was considered to be of insufficient quality, this left: 286 Controls (aged 34 [SD 9.5]  
1064 years, 46% women), 161 Schizophrenics (aged 32 [SD 8.8] years, 35% women) and  
1065 189 participants with Bipolar Disorder (aged 34 [SD 11.5] years, 58% women).  
1066 Patients were recruited from the psychiatric unit of Oslo University Hospital and were  
1067 assessed for psychiatric illness with the Structural Clinical Interview for DSM-IV Axis  
1068 I disorders (SCID-I). This assessment was either administered by an MD, or a  
1069 clinically trained psychologist, and was used to assess the presence of AXIS I  
1070 disorders. Before participation, control participants were screened to exclude serious  
1071 somatic and psychiatric illness, substance abuse, or MRI-incompatibility. All  
1072 participants gave written informed consent before participation. Further information  
1073 about this sample and the scan protocols used can be found in Rimol, L. M. et al<sup>78</sup>.  
1074 We did not use any statistical methods to pre-define the sample size used in this  
1075 investigation. Nevertheless, the sample used is among the largest of any  
1076 investigating structural brain alterations in Schizophrenia<sup>79</sup> and Bipolar disorder<sup>41</sup>

### 1077 **ADHD sample**

1078 Data for the ADHD sample was taken from the NeuroIMAGE project, a clinical cohort  
1079 study. The study is made up of individuals tested at two different sites in the  
1080 Netherlands, The Donders Centre for Cognitive Neuroimaging in Nijmegen, and the  
1081 Vrije Universiteit in Amsterdam. The total sample consisted of 184 participants  
1082 suffering from ADHD, 103 unaffected siblings, and 128 healthy controls. Further  
1083 information on the participants and the protocols used can be found in von Rhein et  
1084 al<sup>80</sup>. This sample includes a number of very young participants, which is likely to  
1085 introduce a large degree of heterogeneity into the analysis. For this reason, we did  
1086 not analyse the data from participants under the age of fifteen. This age divide point

1087 was considered to offer a reasonable trade-off between sample homogeneity and  
1088 size. The data for 12 of the participants was not used as it was deemed to be of  
1089 insufficient quality. Case-control Analyses were made between 74 healthy controls  
1090 (aged 18 [SD 2.0] years, 50% women) and 131 ADHD participants (aged 18 [SD 2.3]  
1091 years, 27% women). No formal statistical methods were used to determine the size  
1092 of this sample. However, this sample is large compared to similar samples  
1093 investigating case-control differences in brain structure in patients with ADHD<sup>81</sup>.

1094

1095

1096

1097

1098

#### 1099 **Data Availability Statement**

1100 IMAGEN data used in this investigation will be made available upon reasonable  
1101 request to the corresponding author. All other data is available upon reasonable  
1102 request addressed to the appropriate study leads.

1103

#### 1104 **Code Availability Statement**

1105 The core code used to run the analyses reported in this study are available as  
1106 Supplementary Software. Supporting code can be found at:  
1107 <https://github.com/alexjamesing/mscca-regression-code>.

1108

1109

1110

1111

1112

1113

1114

1115

1116

1117

1118

1119

1120

1121

1122

1123 **References**

1124

1125 1. Kessler RC, Amminger GP, Aguilar-Gaxiola S, Alonso J, Lee S, Ustun TB. Age of onset of mental  
1126 disorders: A review of recent literature. *Curr Opin Psychiatry*. 2007;20(4):359-364.

1127 2. Giedd JN, Blumenthal J, Jeffries NO, et al. Brain development during childhood and adolescence: A  
1128 longitudinal MRI study. *Nat Neurosci*. 1999;2(10):861-863.

1129 3. Steinberg L. Risk taking in adolescence: New perspectives from brain and behavioral science.

1130 *Current directions in psychological science*. 2007;16(2):55-59.

- 1131 4. Gogtay N, Giedd JN, Lusk L, et al. Dynamic mapping of human cortical development during  
1132 childhood through early adulthood. *Proc Natl Acad Sci U S A*. 2004;101(21):8174-8179.
- 1133 5. Drysdale AT, Grosenick L, Downar J, et al. Resting-state connectivity biomarkers define  
1134 neurophysiological subtypes of depression. *Nat Med*. 2016.
- 1135 6. Insel T, Cuthbert B, Garvey M, et al. No title. *Research domain criteria (RDoC): toward a new*  
1136 *classification framework for research on mental disorders*. 2010.
- 1137 7. Lahey BB, Applegate B, Hakes JK, Zald DH, Hariri AR, Rathouz PJ. Is there a general factor of  
1138 prevalent psychopathology during adulthood? *J Abnorm Psychol*. 2012;121(4):971.
- 1139 8. Zhang X, Mormino EC, Sun N, et al. Bayesian model reveals latent atrophy factors with dissociable  
1140 cognitive trajectories in alzheimer's disease. *Proc Natl Acad Sci U S A*. 2016;113(42):E6544.
- 1141 9. Rosenberg MD, Finn ES, Scheinost D, et al. A neuromarker of sustained attention from whole-  
1142 brain functional connectivity. *Nat Neurosci*. 2016;19(1):165.
- 1143 10. Smith SM, Nichols TE, Vidaurre D, et al. A positive-negative mode of population covariation links  
1144 brain connectivity, demographics and behavior. *Nat Neurosci*. 2015;18(11):1565-1567.
- 1145 11. Witten DM, Tibshirani R, Hastie T. A penalized matrix decomposition, with applications to sparse  
1146 principal components and canonical correlation analysis. *Biostatistics*. 2009;10(3):515-534.
- 1147 12. Xia CH, Ma Z, Ciric R, et al. Linked dimensions of psychopathology and connectivity in functional  
1148 brain networks. *Nature communications*. 2018;9(1):3003.
- 1149 14. Goodman R, Ford T, Richards H, Gatward R, Meltzer H. The development and well-being  
1150 assessment: Description and initial validation of an integrated assessment of child and adolescent  
1151 psychopathology. *Journal of child psychology and psychiatry*. 2000;41(05):645-655.
- 1152 15. Ashburner J. A fast diffeomorphic image registration algorithm. *Neuroimage*. 2007;38(1):95-113.
- 1153 16. Smith SM, Jenkinson M, Johansen-Berg H, et al. Tract-based spatial statistics: Voxelwise analysis  
1154 of multi-subject diffusion data. *Neuroimage*. 2006;31(4):1487-1505.



- 1155 17. Miller KL, Alfaro-Almagro F, Bangerter NK, et al. Multimodal population brain imaging in the UK  
1156 biobank prospective epidemiological study. *Nat Neurosci*. 2016;19(11):1523.
- 1157 18. Ashburner J, Friston KJ. Voxel-based morphometry—the methods. *Neuroimage*. 2000;11(6):805-  
1158 821.
- 1159 19. Smith SM, Jenkinson M, Johansen-Berg H, et al. Tract-based spatial statistics: Voxelwise analysis  
1160 of multi-subject diffusion data. *Neuroimage*. 2006;31(4):1487-1505.
- 1161 20. Power JD, Fair DA, Schlaggar BL, Petersen SE. The development of human functional brain  
1162 networks. *Neuron*. 2010;67(5):735-748.
- 1163 21. Meinshausen N, Bühlmann P. Stability selection. *Journal of the Royal Statistical Society: Series B*  
1164 *(Statistical Methodology)*. 2010;72(4):417-473.
- 1165 22. Schmaal L, Hibar DP, Sämann PG, et al. Cortical abnormalities in adults and adolescents with  
1166 major depression based on brain scans from 20 cohorts worldwide in the ENIGMA major depressive  
1167 disorder working group. *Mol Psychiatry*. 2016.
- 1168 23. Chen G, Hu X, Li L, et al. Disorganization of white matter architecture in major depressive  
1169 disorder: A meta-analysis of diffusion tensor imaging with tract-based spatial statistics. *Scientific*  
1170 *reports*. 2016;6:21825.
- 1171 24. Guo W, Liu F, Liu J, et al. Increased cerebellar-default-mode-network connectivity in drug-naïve  
1172 major depressive disorder at rest. *Medicine*. 2015;94(9).
- 1173 25. Carmona S, Vilarroya O, Bielsa A, et al. Global and regional gray matter reductions in ADHD: A  
1174 voxel-based morphometric study. *Neurosci Lett*. 2005;389(2):88-93.
- 1175 26. Krueger RF, Caspi A, Moffitt TE, Silva PA. The structure and stability of common mental disorders  
1176 (DSM-III-R): A longitudinal-epidemiological study. *J Abnorm Psychol*. 1998;107(2):216.
- 1177 27. Diedenhofen B, Musch J. Cocor: A comprehensive solution for the statistical comparison of  
1178 correlations. *PLoS one*. 2015;10(4):e0121945.

- 1179 28. Dunn OJ, Clark V. Correlation coefficients measured on the same individuals. *Journal of the*  
1180 *American Statistical Association*. 1969;64(325):366-377.
- 1181 29. Whelan R, Watts R, Orr CA, et al. Neuropsychosocial profiles of current and future adolescent  
1182 alcohol misusers. *Nature*. 2014;512(7513):185-189.
- 1183 30. Lahey BB, Van Hulle CA, Singh AL, Waldman ID, Rathouz PJ. Higher-order genetic and  
1184 environmental structure of prevalent forms of child and adolescent psychopathology. *Arch Gen*  
1185 *Psychiatry*. 2011;68(2):181-189.
- 1186 31. Kessler RC, Angermeyer M, Anthony JC, et al. Lifetime prevalence and age-of-onset distributions  
1187 of mental disorders in the world health organization's world mental health survey initiative. *World*  
1188 *Psychiatry*. 2007;6(3):168-176.
- 1189 32. Mayberg HS. Modulating dysfunctional limbic-cortical circuits in depression: Towards  
1190 development of brain-based algorithms for diagnosis and optimised treatment. *Br Med Bull*.  
1191 2003;65(1):193-207.
- 1192 33. Witelson SF. Hand and sex differences in the isthmus and genu of the human corpus callosum: A  
1193 postmortem morphological study. *Brain*. 1989;112(3):799-835.
- 1194 34. Tham MW, San Woon P, Sum MY, Lee T, Sim K. White matter abnormalities in major depression:  
1195 Evidence from post-mortem, neuroimaging and genetic studies. *J Affect Disord*. 2011;132(1-2):26-36.
- 1196 35. Chen G, Hu X, Li L, et al. Disorganization of white matter architecture in major depressive  
1197 disorder: A meta-analysis of diffusion tensor imaging with tract-based spatial statistics. *Scientific*  
1198 *reports*. 2016;6:21825.
- 1199 36. Raichle ME, MacLeod AM, Snyder AZ, Powers WJ, Gusnard DA, Shulman GL. A default mode of  
1200 brain function. *Proceedings of the National Academy of Sciences*. 2001;98(2):676-682.
- 1201 37. Buckner RL, Andrews-Hanna JR, Schacter DL. The brain's default network. *Ann N Y Acad Sci*.  
1202 2008;1124(1):1-38.

- 1203 38. Ray RD, Ochsner KN, Cooper JC, Robertson ER, Gabrieli JD, Gross JJ. Individual differences in trait  
1204 rumination and the neural systems supporting cognitive reappraisal. *Cognitive, Affective, &*  
1205 *Behavioral Neuroscience*. 2005;5(2):156-168.
- 1206 39. Stoodley CJ. The cerebellum and cognition: Evidence from functional imaging studies. *The*  
1207 *Cerebellum*. 2012;11(2):352-365.
- 1208 40. Guggenmos M, Schmack K, Sekutowicz M, et al. Quantitative neurobiological evidence for  
1209 accelerated brain aging in alcohol dependence. *Translational psychiatry*. 2017;7(12):1279.
- 1210 41. Hibar DP, Westlye LT, Doan NT, et al. Cortical abnormalities in bipolar disorder: An MRI analysis  
1211 of 6503 individuals from the ENIGMA bipolar disorder working group. *Mol Psychiatry*. 2017.
- 1212 42. McGorry PD, Hickie IB, Yung AR, Pantelis C, Jackson HJ. Clinical staging of psychiatric disorders: A  
1213 heuristic framework for choosing earlier, safer and more effective interventions. *Aust N Z J*  
1214 *Psychiatry*. 2006;40(8):616-622.
- 1215 43. Biswal B, Zerrin Yetkin F, Houghton VM, Hyde JS. Functional connectivity in the motor cortex of  
1216 resting human brain using echo-planar MRI. *Magnetic resonance in medicine*. 1995;34(4):537-541.
- 1217 44. Schumann G, Loth E, Banaschewski T, et al. The IMAGEN study: Reinforcement-related behaviour  
1218 in normal brain function and psychopathology. *Mol Psychiatry*. 2010;15(12):1128-1139.
- 1219 45. Goodman R. The strengths and difficulties questionnaire: A research note. *Journal of child*  
1220 *psychology and psychiatry*. 1997;38(5):581-586.
- 1221 46. Vulser H, Lemaitre H, Artiges E, et al. Subthreshold depression and regional brain volumes in  
1222 young community adolescents. *Journal of the American Academy of Child & Adolescent Psychiatry*.  
1223 2015;54(10):832-840.
- 1224 47. Ashburner J, Friston KJ. Unified segmentation. *Neuroimage*. 2005;26(3):839-851.

- 1225 48. Grellmann C, Bitzer S, Neumann J, et al. Comparison of variants of canonical correlation analysis  
1226 and partial least squares for combined analysis of MRI and genetic data. *Neuroimage*. 2015;107:289-  
1227 310.
- 1228 49. Jones DK, Williams SCR, Gasston D, Horsfield MA, Simmons A, Howard R. Isotropic resolution  
1229 diffusion tensor imaging with whole brain acquisition in a clinically acceptable time. *Hum Brain*  
1230 *Mapp*. 2002;15(4):216-230.
- 1231 50. Smith SM, Jenkinson M, Woolrich MW, et al. Advances in functional and structural MR image  
1232 analysis and implementation as FSL. *Neuroimage*. 2004;23:S219.
- 1233 51. Avants BB, Tustison NJ, Song G, Cook PA, Klein A, Gee JC. A reproducible evaluation of ANTs  
1234 similarity metric performance in brain image registration. *Neuroimage*. 2011;54(3):2033-2044.
- 1235 52. Pruim RH, Mennes M, van Rooij D, Llera A, Buitelaar JK, Beckmann CF. ICA-AROMA: A robust ICA-  
1236 based strategy for removing motion artifacts from fMRI data. *Neuroimage*. 2015;112:267-277.
- 1237 53. Pruim RH, Mennes M, Buitelaar JK, Beckmann CF. Evaluation of ICA-AROMA and alternative  
1238 strategies for motion artifact removal in resting state fMRI. *Neuroimage*. 2015;112:278-287.
- 1239 54. Behzadi Y, Restom K, Liao J, Liu TT. A component based noise correction method (CompCor) for  
1240 BOLD and perfusion based fMRI. *Neuroimage*. 2007;37(1):90-101.
- 1241 55. Fischl B. FreeSurfer. *Neuroimage*. 2012;62(2):774-781.
- 1242 56. Power JD, Cohen AL, Nelson SM, et al. Functional network organization of the human brain.  
1243 *Neuron*. 2011;72(4):665-678.
- 1244 57. Hotelling H. Relations between two sets of variates. *Biometrika*. 1936:321-377.
- 1245 58. Witten DM, Tibshirani RJ. Extensions of sparse canonical correlation analysis with applications to  
1246 genomic data. *Statistical applications in genetics and molecular biology*. 2009;8(1):1-27.
- 1247 59. Parkhomenko E, Tritchler D, Beyene J. Sparse canonical correlation analysis with application to  
1248 genomic data integration. *Statistical Applications in Genetics and Molecular Biology*. 2009;8(1):1-34.

- 1249 60. Gifi A. *Nonlinear multivariate analysis*. John Wiley & Sons Incorporated; 1990.
- 1250 61. Jenkins LM, Barba A, Campbell M, et al. Shared white matter alterations across emotional  
1251 disorders: A voxel-based meta-analysis of fractional anisotropy. *NeuroImage: Clinical*. 2016;12:1022-  
1252 1034.
- 1253 62. Goodkind M, Eickhoff SB, Oathes DJ, et al. Identification of a common neurobiological substrate  
1254 for mental illness. *JAMA psychiatry*. 2015;72(4):305-315.
- 1255 63. Everitt BS, Dunn G. *Applied multivariate data analysis*. Vol 2. Arnold London; 2001.
- 1256 64. Timm NH, Carlson JE. Part and bipartial canonical correlation analysis. *Psychometrika*.  
1257 1976;41(2):159-176.
- 1258 65. O'Brien LM, Ziegler DA, Deutsch CK, Frazier JA, Herbert MR, Locascio JJ. Statistical adjustments  
1259 for brain size in volumetric neuroimaging studies: Some practical implications in methods. *Psychiatry*  
1260 *Research: Neuroimaging*. 2011;193(2):113-122.
- 1261 66. Pell GS, Briellmann RS, Chan CHP, Pardoe H, Abbott DF, Jackson GD. Selection of the control  
1262 group for VBM analysis: Influence of covariates, matching and sample size. *Neuroimage*.  
1263 2008;41(4):1324-1335.
- 1264 67. Voevodskaya O, Simmons A, Nordenskjöld R, et al. The effects of intracranial volume adjustment  
1265 approaches on multiple regional MRI volumes in healthy aging and alzheimer's disease. *Frontiers in*  
1266 *aging neuroscience*. 2014;6.
- 1267 68. Van Den Wollenberg, Arnold L. Redundancy analysis an alternative for canonical correlation  
1268 analysis. *Psychometrika*. 1977;42(2):207-219.
- 1269 69. Stewart D, Love W. A general canonical correlation index. *Psychol Bull*. 1968;70(3):160-163.
- 1270 70. Monteiro JM, Rao A, Shawe-Taylor J, Mourão-Miranda J, Alzheimer's Disease Initiative. A  
1271 multiple hold-out framework for sparse partial least squares. *J Neurosci Methods*. 2016;271:182-194.

- 1272 71. Holmes AP, Blair RC, Watson G, Ford I. Nonparametric analysis of statistic images from functional  
1273 mapping experiments. *Journal of Cerebral Blood Flow & Metabolism*. 1996;16(1):7-22.
- 1274 72. Westfall PH, Troendle JF. Multiple testing with minimal assumptions. *Biometrical Journal*.  
1275 2008;50(5):745-755.
- 1276 73. Westfall PH, Young SS. *Resampling-based multiple testing: Examples and methods for p-value*  
1277 *adjustment*. Vol 279. John Wiley & Sons; 1993.
- 1278 74. Friedman J, Hastie T, Tibshirani R. *The elements of statistical learning*. Vol 1. Springer series in  
1279 statistics New York; 2001.
- 1280 75. Aebi M, Kuhn C, Metzke CW, Stringaris A, Goodman R, Steinhausen H. The use of the  
1281 development and well-being assessment (DAWBA) in clinical practice: A randomized trial. *Eur Child*  
1282 *Adolesc Psychiatry*. 2012;21(10):559-567.
- 1283 76. Steinberg L. Cognitive and affective development in adolescence. *Trends Cogn Sci (Regul Ed)*.  
1284 2005;9(2):69-74.
- 1285 77. Schmaal L, Veltman DJ, van Erp TG, et al. Subcortical brain alterations in major depressive  
1286 disorder: Findings from the ENIGMA major depressive disorder working group. *Mol Psychiatry*.  
1287 2016;21(6):806.
- 1288 78. Rimol LM, Nesvåg R, Hagler DJ, et al. Cortical volume, surface area, and thickness in  
1289 schizophrenia and bipolar disorder. *Biol Psychiatry*. 2012;71(6):552-560.
- 1290 79. van Erp TG, Hibar DP, Rasmussen JM, et al. Subcortical brain volume abnormalities in 2028  
1291 individuals with schizophrenia and 2540 healthy controls via the ENIGMA consortium. *Mol*  
1292 *Psychiatry*. 2016;21(4):547.
- 1293 80. von Rhein D, Mennes M, van Ewijk H, et al. The NeuroIMAGE study: A prospective phenotypic,  
1294 cognitive, genetic and MRI study in children with attention-deficit/hyperactivity disorder. design and  
1295 descriptives. *Eur Child Adolesc Psychiatry*. 2015;24(3):265-281.

1296 81. Hoogman M, Bralten J, Hibar DP, et al. Subcortical brain volume differences in participants with  
1297 attention deficit hyperactivity disorder in children and adults: A cross-sectional mega-analysis. *The*  
1298 *Lancet Psychiatry*. 2017;4(4):310-319.

1299

1300

1301

1302

1303

1304

1305

1306

1307

1308

1309

1310

1311

## 1312 **Acknowledgments**

1313 This work received support from the following sources: the European Union-funded FP6 Integrated  
1314 Project IMAGEN (Reinforcement-related behaviour in normal brain function and psychopathology)  
1315 (LSHM-CT- 2007-037286), the Horizon 2020 funded ERC Advanced Grant 'STRATIFY' (Brain network  
1316 based stratification of reinforcement-related disorders) (695313), ERANID (Understanding the  
1317 Interplay between Cultural, Biological and Subjective Factors in Drug Use Pathways) (PR-ST-0416-  
1318 10004), BRIDGET (JPND: BRain Imaging, cognition Dementia and next generation GENomics)  
1319 (MR/N027558/1), Human Brain Project (HBP SGA 2, 785907), the FP7 project MATRICS (603016), the  
1320 Medical Research Council Grant 'c-VEDA' (Consortium on Vulnerability to Externalizing Disorders and  
1321 Addictions) (MR/N000390/1), the National Institute for Health Research (NIHR) Biomedical Research  
1322 Centre at South London and Maudsley NHS Foundation Trust and King's College London, the  
1323 Bundesministerium für Bildung und Forschung (BMBF grants 01GS08152; 01EV0711; Forschungsnetz  
1324 AERIAL 01EE1406A, 01EE1406B , 01ZX1314G, 01GS08147), the Deutsche Forschungsgemeinschaft  
1325 (DFG grants SM 80/7-2, SFB 940/2), the Medical Research Foundation and Medical Research Council  
1326 (grants MR/R00465X/1 and MR/S020306/1), the National Institutes of Health (NIH) funded ENIGMA  
1327 (grants 5U54EB020403-05 and 1R56AG058854-01). Further support was provided by grants from:  
1328 ANR (project AF12-NEUR0008-01 - WM2NA, and ANR-12-SAMA-0004), the Fondation de France, the  
1329 Fondation pour la Recherche Médicale, the Mission Interministérielle de Lutte-contre-les-Drogues-  
1330 et-les-Conduites-Addictives (MILDECA), the Assistance-Publique-Hôpitaux-de-Paris and INSERM  
1331 (interface grant), Paris Sud University IDEX 2012; the National Institutes of Health, Science  
1332 Foundation Ireland (16/ERC/3797), U.S.A. (Axon, Testosterone and Mental Health during  
1333 Adolescence; RO1 MH085772-01A1), and by NIH Consortium grant U54 EB020403, supported by a

1334 cross-NIH alliance that funds Big Data to Knowledge Centres of Excellence. AFM gratefully  
1335 acknowledges funding from the Netherlands Organisation for Scientific Research via the  
1336 Vernieuwingsimpuls VIDI programme (grant number 016.156.415). The funders had no role in study  
1337 design, data collection and analysis, decision to publish, or preparation of the manuscript  
1338  
1339

#### 1340 **Author Contributions**

#### 1341 **Author Contributions**

1342 **Pre-processed data:** AI, CC, IMV, PGS, HL, TJ, GR; **Analysed the data:** AI, PGS; **Wrote the manuscript:**  
1343 AI, GS, FB, PGS; **Conceptualised the study:** AI, GS, TWR, AM, JA, EB; **Collected Data:** NT, EBQ, TW,  
1344 SD, TB, ALWB, UB, CB, PC, TF, HF, VF, HG, PS, PG, YG, AH, BI, VK, JLM, AML, SB, FN, BVN, DPO, MLPM,  
1345 SM, JP, LP, MS, AS, MNS, HW, RW, OAA, IA, EDB, JB; **Prepared Figures:** AI, NT **Revised Manuscript:**  
1346 All Authors

1347

#### 1348 **Competing Interests**

1349 Dr. Banaschewski served in an advisory or consultancy role for Lundbeck, Medice, Neurim  
1350 Pharmaceuticals, Oberberg GmbH, Shire. He received conference support or speaker's fee  
1351 by Lilly, Medice, Novartis and Shire. He has been involved in clinical trials conducted by Shire  
1352 & Viforpharma. He received royalties from Hogrefe, Kohlhammer, CIP Medien, Oxford  
1353 University Press. The present work is unrelated to the above grants and relationships. Dr.  
1354 Barker has received honoraria from General Electric Healthcare for teaching on scanner  
1355 programming courses and acts as a consultant for IXICO. Dr. Andreassen received speaker's  
1356 honorarium from Lundbeck. Gabriel Robert received financial support from scientific  
1357 meetings (Janssen & Janssen, Otsuka-Lundbeck). Dr. Meyer-Lindenberg has received  
1358 consultant fees from Boehringer Ingelheim, Brainsway, Elsevier, Lundbeck Int. Neuroscience  
1359 Foundation and Science Advances. The other authors report no biomedical financial  
1360 interests or potential conflicts of interest.

1361 *Figure 1: Results of the first msCCA-regression analysis showing relations between*  
1362 *anxiety/depression psychiatric symptoms and neuroimaging measures in the IMAGEN sample. (a):*  
1363 *The full msCCA-regression model linking psychiatric symptoms to VBM, TBSS and rs-fcMRI*  
1364 *neuroimaging measures at age 19. We found associations between psychiatric symptoms and*  
1365 *neuroimaging measures of  $r = 0.59(465)$  ( $p < 0.001$ ) in the training set, and associations between*  
1366 *symptoms and the brain of  $r=0.23(197)$ ,  $p<0.001$ , 95% CIs= $0.13, \infty$  in the test set; (b): Shows the*  
1367 *msCCA-regression model linking psychiatric symptoms with the different neuroimaging measures (c):*  
1368 *Psychiatric symptoms contributing to this relation are shown on the left, their canonical weights are*  
1369 *shown in red. (d): rs-fcMRI measures of functional connectivity. (e): VBM measures of grey matter*  
1370 *volume associated with symptoms. (f): TBSS measures of fractional anisotropy (FA).*

1371

1372 *Figure 2: Results of the second msCCA-regression analyses showing relations between executive*  
1373 *dysfunction symptoms and neuroimaging measures in the IMAGEN sample, following the removal of*  
1374 *the first canonical relation. (a): The full msCCA-regression model linking psychiatric symptoms to*  
1375 *VBM, TBSS and rs-fcMRI neuroimaging measures at age 19. We found associations between*  
1376 *executive dysfunction symptoms and neuroimaging measures of  $r = 0.46$  ( $p = 0.004$ ) in the training*  
1377 *set, and associations between symptoms and the brain of  $r = 0.19(197)$ ,  $p = 0.002$ , 95% CIs = $0.087,$   
1378  $\infty$  in the test set; (b) msCCA-regression model linking psychiatric symptoms with the different  
1379 neuroimaging measures (c) Symptoms contributing to this relation are shown on the left their  
1380 canonical weights are shown in red. (d) rs-fcMRI measures of functional connectivity. (e) VBM*



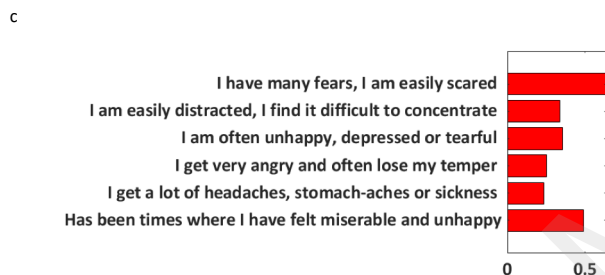
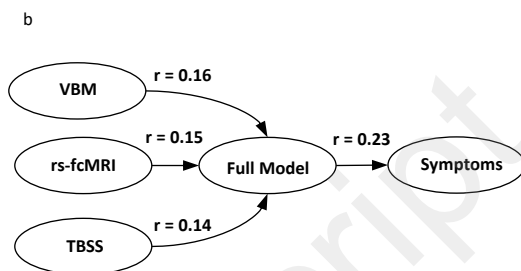
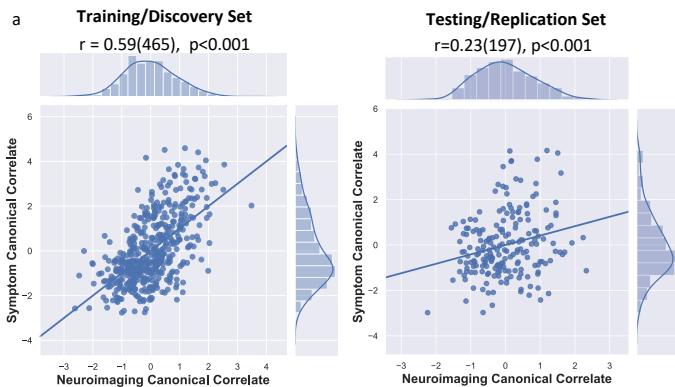
1381 measures of grey matter volume associated with symptoms. (f): TBSS measures of fractional  
1382 anisotropy (FA).  
1383

1384 *Figure 3: Longitudinal analysis of canonical correlates. (a) anxiety/depression symptom correlates:*  
1385 *VBM and TBSS brain correlates established at age 19 are associated with anxiety/depression*  
1386 *behavioural symptoms at age 19 ( $r = 0.19(180)$ ,  $p = 0.003$ , 95% CIs= $0.069, \infty$ ), but not at age 14*  
1387 *( $r=0.020(180)$ ,  $p=0.40$ , 95% CIs= $-0.10, \infty$ ). Brain correlates at 14 years predict the manifestation of*  
1388 *behavioral symptoms at 19 years ( $r=0.14(180)$ ,  $p=0.023$ , 95% CIs= $0.022, \infty$ ). (b) Executive*  
1389 *dysfunction symptom correlates: VBM and TBSS correlates established at age 19 are associated with*  
1390 *behavioral symptoms at age 19 ( $r = 0.15(180)$ ,  $p = 0.024$ , 95% CIs= $0.028, \infty$ ), but not at age 14*  
1391 *( $r=0.030(180)$ ,  $p=0.41$ , 95% CIs= $-0.093, \infty$ ). Brain correlates at 14 years do not predict the*  
1392 *manifestation of behavioral symptoms at 19 years ( $r=0.11(180)$ ,  $p=0.065$ , 95% CIs = $-0.010, \infty$ ).*

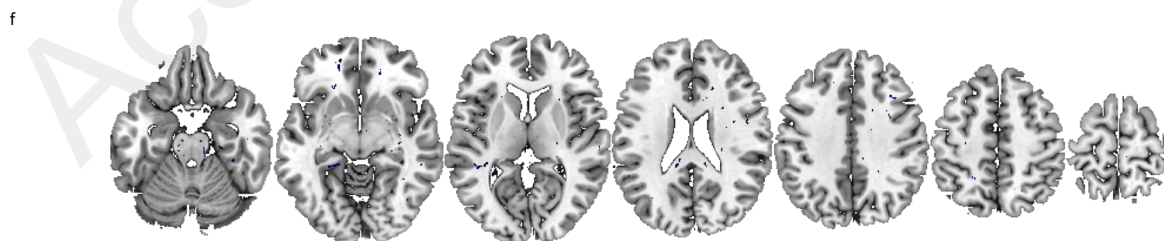
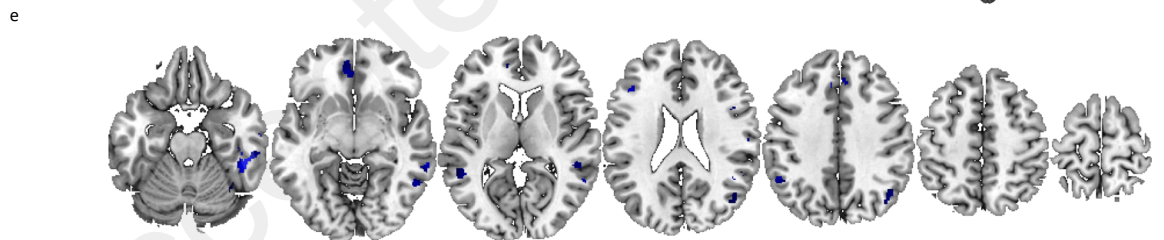
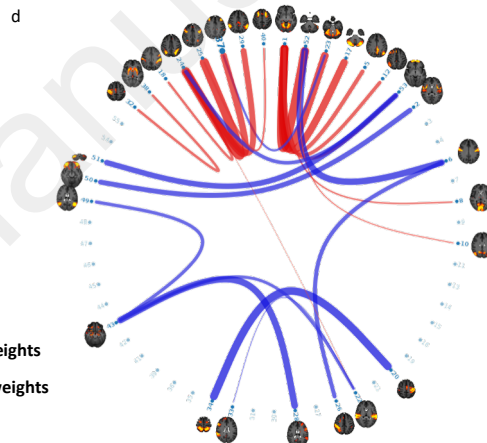
1393  
1394

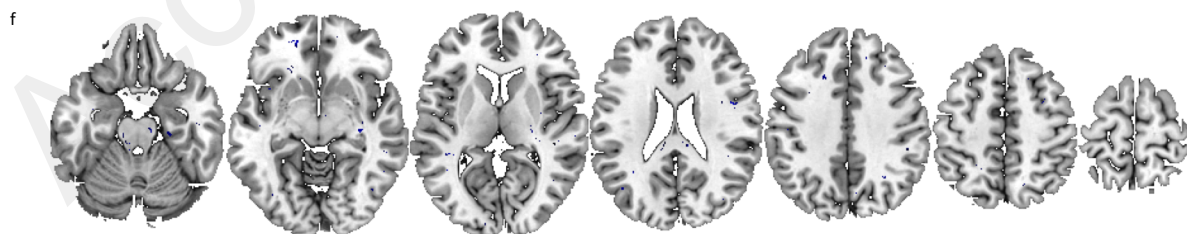
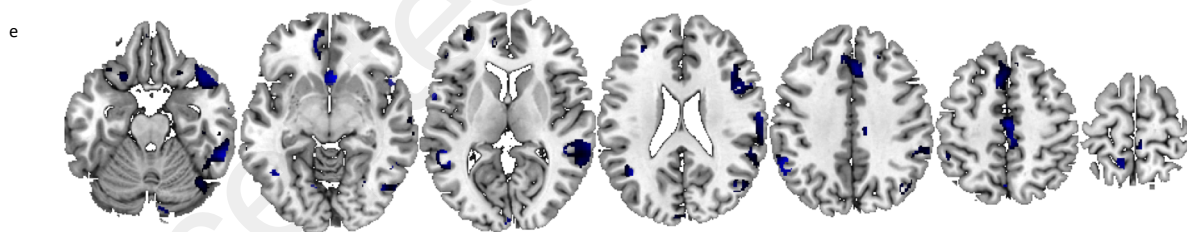
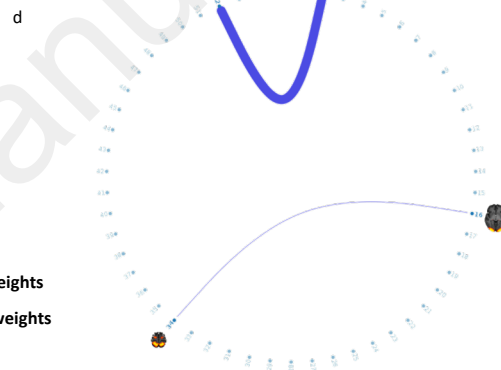
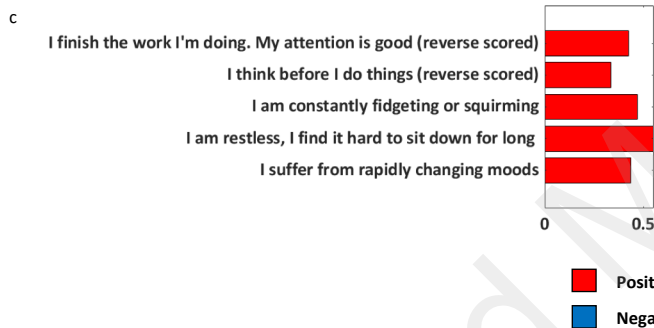
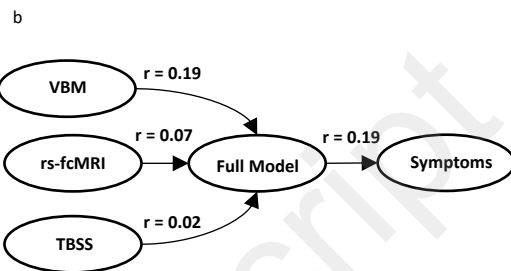
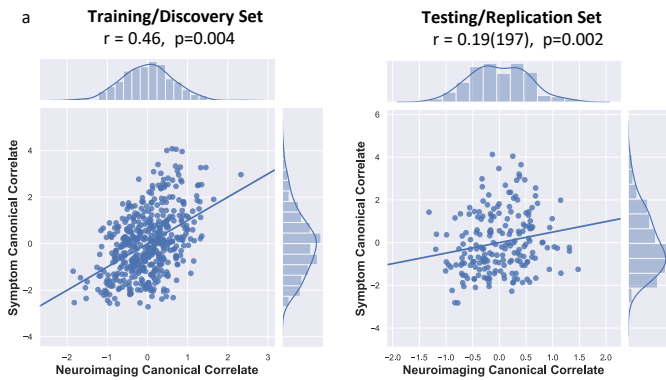
1395 *Figure 4: Differences in the grey matter correlates of anxiety/depression and executive dysfunction*  
1396 *psychiatric symptoms, between cases and controls for a range of psychiatric illnesses. For the box*  
1397 *and whisker plots, the central mark in each box represents the median, with the top and bottom edges*  
1398 *of the box indicating the 25th and 75th percentiles of the sample respectively, whiskers represent 1.5x*  
1399 *the interquartile range and the hollow circles represent sample outliers. For display purposes, total*  
1400 *grey matter in each case-control comparison is divided by the pooled standard deviation. The effect*  
1401 *sizes (calculated using Cohen's D) relating to these differences are shown in the right-hand panel. (a):*  
1402 *Differences in grey matter volume between patients and controls in the anxiety/depression set of grey*  
1403 *matter correlates are shown in the left-hand panel. Clinical psychiatric disorders exhibited the*  
1404 *following case-control differences: Depression:  $t$ -statistic= $4.61(612)$ ,  $p < 0.001$ , Cohen's  $D = 0.39$ , 95%*  
1405 *CIs= $0.25, \infty$ ; Schizophrenia:  $t$ -statistic= $2.54(445)$ ,  $p=0.002$ , Cohen's  $D=0.25$ , 95% CIs =  $0.087, \infty$ ;*  
1406 *ADHD ( $t$ -statistic= $1.84(203)$ ,  $p=0.034$ , Cohen's  $D=0.26$ , 95% CIs= $0.030, \infty$ ; Bipolar: ( $t$ -statistic= $-$*   
1407  *$0.23(473)$ ,  $p=0.59$ , Cohen's  $D=-0.02$ , 95% CIs= $-0.17, \infty$ ). (b): Differences in grey matter volume*  
1408 *between patients and controls in the executive dysfunction set of grey matter correlates. Clinical*  
1409 *psychiatric disorders exhibited the following case-control differences: Depression:  $t$ -*  
1410 *statistic= $1.65(612)$ ,  $p=0.050$ , Cohen's  $D=0.14$ , 95% CIs= $0.001, \infty$ , Schizophrenia:  $t$ -*  
1411 *statistic= $2.81(445)$ ,  $p=0.0026$ , Cohen's  $D=0.28$ , 95% CIs= $0.11, \infty$ ; ADHD:  $t$ -statistic= $2.19(203)$ ,*  
1412  *$p=0.014$ , Cohen's  $D=0.32$ , 95% CIs= $0.070, \infty$ ; Bipolar:  $t$ -statistic= $-1.33(473)$ ,  $p=0.90$ , Cohen's  $D=-$*   
1413  *$0.12$ , 95% CIs= $-0.27, \infty$ .*

1414  
1415  
1416



■ Positive weights  
■ Negative weights





a.

**Anxiety/Depression**

$r = 0.19(180), p = 0.003$

Age 19

Symptoms

Neuroimaging

$r = 0.14(180), p = 0.023$

Age 14

Symptoms

Neuroimaging

$r = 0.020(180), p = 0.40$

b.

**Executive Dysfunction**

$r = 0.15(180), p = 0.024$

Symptoms

Neuroimaging

$r = 0.11(180), p = 0.065$

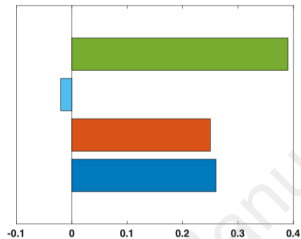
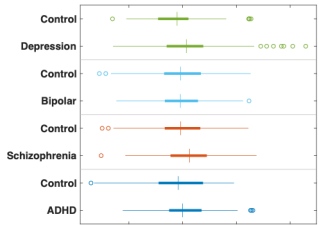
Symptoms

Neuroimaging

$r = 0.030(180), p = 0.41$

Accepted Manuscript

a.



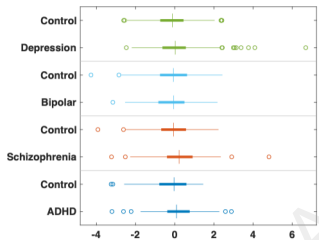
t-statistic=4.61(612),  $p < 0.001$ , Cohen's D = 0.39

t-statistic=-0.23(473),  $p = 0.59$ , Cohen's D=-0.02

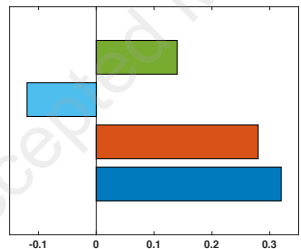
t-statistic=2.54(445),  $p = 0.002$ , Cohen's D=0.25

t-statistic=1.84(203),  $p = 0.034$ , Cohen's D=0.26

b.



**Normalised Grey Matter**



**Cohen's D**

t-statistic=1.65(612),  $p = 0.050$ , Cohen's D=0.14

t-statistic=-1.33(473),  $p = 0.90$ , Cohen's D=-0.12

t-statistic=2.81(445),  $p = 0.0026$ , Cohen's D=0.28

t-statistic=2.19(203),  $p = 0.014$ , Cohen's D=0.32